OPEN ACCESS

International Journal of Biotechnology and Molecular Biology Research

July-December 2022
ISSN 2141-2154
DOI: 10.5897/IJBMBR
www.academicjournals.org

ACADEMIC JOURNALS
expand your knowledge

About IJBMBR

The International Journal of Biotechnology and Molecular Biology Research (IJBMBR) is a peer reviewed open access journal. The journal commenced publication in March 2010.

The main objective of the journal is to bring the latest developments in the field of biotechnology and molecular biology to researchers. The journal publishes original research articles, review papers and short communications, covering all aspects of biotechnology and molecular biology. The scope includes: Molecular Biology, Biotechnology, Microbial technology, Molecular immunology, System Biology, Agricultural biotechnology, Industrial biotechnology, Bioinformatics and computational biology, Medical and pharmaceutical biotechnology, Chemical and metabolic engineering and Genomics.

Open Access Policy

Open Access is a publication model that enables the dissemination of research articles to the global community without any form of restriction. All articles published under open access can be accessed by anyone with internet connection.

The International Journal of Biotechnology and Molecular Biology Research is an Open Access journal. Abstracts and full texts of all articles published in this journal are freely accessible to everyone immediately after publication without any form of restriction.

Please see journal archive for all past issues or see all published articles

Article License

All articles published by the International Journal of Biotechnology and Molecular Biology Research are licensed under the Creative Commons Attribution 4.0 International License. This permits anyone to copy, redistribute, remix, transmit and adapt the work provided the original work and source is appropriately cited. Citation should include the article's DOI. The article license is displayed both on the abstract page and the full-text PDF of each article.

Please see more details about Creative Commons Attribution License 4.0

Article Copyright

When an article is published in the journal, the author(s) of the article retain the copyright. Author(s) may republish the article as part of a book or other materials.

A copyright statement is displayed both on the abstract page and the full-text PDF of each article.

Example: Copyright ©2016 Author(s) retains the copyright of this article.

Memberships and Standards

Academic Journals strongly supports the Open Access initiative. Abstracts and full texts of all articles published by Academic Journals are freely accessible to everyone immediately after publication.

All articles published by Academic Journals are licensed under the Creative Commons Attribution 4.0 International License (CC BY 4.0). This permits anyone to copy, redistribute, remix, transmit and adapt the work provided the original work and source is appropriately cited.

Crossref is an association of scholarly publishers that developed Digital Object Identification (DOI) system for the unique identification published materials. Academic Journals is a member of Crossref and uses the DOI system. All articles published by Academic Journals are issued DOI.

Similarity Check powered by iThenticate is an initiative started by CrossRef to help its members actively engage in efforts to prevent scholarly and professional plagiarism. Academic Journals is a member of Similarity Check.

CrossRef Cited-by Linking (formerly Forward Linking) is a service that allows you to discover how your publications are being cited and to incorporate that information into your online publication platform. Academic Journals is a member of CrossRef Cited-by.

Academic Journals is a member of the International Digital Publishing Forum (IDPF). The IDPF is the global trade and standards organization dedicated to the development and promotion of electronic publishing and content consumption.

Contact

Editorial Office: ijbmbr@academicjournals.org

Help Desk: helpdesk@academicjournals.org

Website: http://www.academicjournals.org/journal/IJBMBR

Submit manuscript online http://ms.academicjournals.org

Academic Journals
73023 Victoria Island, Lagos, Nigeria
ICEA Building, 17th Floor,
Kenyatta Avenue, Nairobi, Kenya.

Editors

Prof. Harrison Atagana
Institute for Science and Technology Education
University of South Africa
South Africa.

Prof. U.C. Banerjee
Department of Pharmaceutical Technology (Biotechnology)
National Institute of Pharmaceutical Education and Research
Punjab,
India.

Dr. Y. Omidi
Faculty of Pharmacy
Research Center for Pharmaceutical Nanotechnology
School of Advanced Biomedical Sciences
Tabriz University of Medical Sciences
Tabriz,
Iran.

Dr. Prasun Kumar
Department of Microbial Biotechnology and Genomics,
CSIR-Institute of Genomics and Integrative Biology,
India

Editorial Board Members

Dr. Fazal Shirazi
MD. Anderson Cancer Center
1515 Holcombe Blvd
Houston, TX-77054

Dr. Ekta Tiwary
Vision Sciences,
University of Alabama at Birmingham
USA.

Dr. Bindiya Sachdev
Biochemistry and Molecular Biophysics
Kansas State University
USA

Dr. Salar Khan
Immunology and Microbial Sciences,
The Scripps Research Institute,
USA.

Dr. Shweta Mehrotra Goyal
Department of Botany,
University Of Delhi, Delhi,
India.

Dr. Wancang Liu
Biotechnology core lab,
National Institute of Diabetes and Digestive and Kidney Diseases, NIH,
U.S.A.

Table of Content

Vol. 12(2) pp. 9-21, July-December 2022
DOI: 10.5897/IJBMBR2021.0325
Article Number:9836DF669364
ISSN 2141-2154
Copyright © 2022
Author(s) retain the copyright of this article
http:// www.academicjournals.org/IJBMBR

ACADEMIC JOURNALS
expand your knowledge

International Journal of Biotechnology and Molecular Biology

Full Length Research Paper

FRET as a tool for the studies of structural changes in full-length bacterial phytochrome, Agp1

Njimona Ibrahim[1,3,4*], Ngah Yayah Emerencia[2], Mfopa Adamou[1] and Nkengazong Lucia[1]

[1]Institute of Medical Research and Medicinal Plants Studies (IMPM), Yaoundé, Cameroon.
[2]District Health Service Bamenda, North West Regional Delegation of Health, Ministry of Health, Cameroon.
[3]Bamenda University Institute of Science and Technology, Bamenda, Cameroon.
[4]Karlsruhe Institute of Science and Technology, Karlsruhe, Germany.

Received 16 November, 2021; Accepted 23, May 2022

Bacteriophytochromes (BphPs) are light-regulated biliprotein photoreceptors widely occurring in bacteria. BphPs exists in two spectral distinct states: the red-light absorbing state (Pr) and the far-red light-absorbing state (Pfr). BphPs are composed of an N-terminal photosensory core module and a light-controlled C-terminal histidine kinase module. The detailed mechanism on how photoconversion, initiated by a light-triggered isomerization of the biliverdin chromophore, is conducted from the N-terminal to the C-terminal domain and how the histidine kinase is modulated is still not clear. In this work Agp1 from *Agrobacterium tumefaciens* is used as a model phytochrome. The method of labeling full-length Agp1 mutants with single accessible Cys residue using fluorescence probes is described. Different absorption spectra showed that neither mutagenesis nor fluorescence labeling exerts significant effects on the photoconversion behavior of various Agp1 mutants. The histidine kinase activity assay revealed that the labeled holoproteins exhibit wild-types like autophosphorylation activity that depends on the Pr and the Pfr state. Fluorescence spectroscopic data suggested that fluorescence resonance energy transfer occurs from the donor Atto495 to the acceptor Atto565 in double-labeled Agp1-A362C, K514C, H554C, R603C, I653C, and V674C mutants. Red light irradiation gave rise to small changes on fluorescence emission intensity in some mutants but in some no remarkable inter-subunit distance changes occurred during the photo-conversion from Pr to Pfr in full-length Agp1. In contrast to double-labeled samples, significant changes in fluorescence intensity were observed in single-labeled samples.

Key words: Bacteriophytochromes (BphPs), C-terminal domain, photosensory, phytochrome.

INTRODUCTION

Phytochromes (Phys) are homodimeric, red/far-red light sensing photoreceptors with a bilin chromophore found in plants, fungi and bacteria. These photoreceptors are composed of the N-terminal photosensory core module and C-terminal output transducing domain. Phys have a characteristic photoconversion between the red-light

*Corresponding author. E-mail: njimona@yahoo.com.

Author(s) agree that this article remain permanently open access under the terms of the Creative Commons Attribution License 4.0 International License

absorbing state (Pr) and far-red absorbing state (Pfr).The chromophore, which is covalently bound via its ring A to a conserved Cys residue of the apoprotein is responsible for this photoconversion behavior. As of plant phytochrome and cyanobacteria phytochrome that uses phytochromobilin (PϕB) and phycocyanobilin (PCB) chromophore, respectively, bacterial phytochromes (Bacteriophytochrome (BphP)) use biliverdin as their chromophore, which is covalently attached to the apoprotein via a thioether linkage to a conserved Cys residue found at the N-terminus of the PAS domain (Bhoo et al., 2001; Giraud and Verméglio, 2008; Davis et al., 1999). BphPs are involved in the regulation of the synthesis of photosynthetic apoprotein, pigmentation, photo-movement and quorum-sensing network (Giraud et al., 2002; Giraud and Verméglio, 2012; Fixen et al., 2014; Barkovits et al., 2011). Structural analysis has revealed that some BphPs are composed of a relatively conserved N-terminal photosensory core module (PCM) and a C-terminal divergent histidine kinase module (HKM). The PCM module is relatively more conserved and is divided into three domains: the PAS (domain denominated after Per/Arnt/Sim), domain followed by the GAF domain (domain denominated after cyclic di-GMP phosphodiesterase/adenyl cyclase/Fhla) and the PHY domain (ddomain-specific for phytochromes). As for the latter this is less conserved than the HKM domain exhibit light-modulated aautophosphorylation activity or reversible phosphotransferase activity in vitro (Yeh et al., 1997; Karniol and Vierstra, 2003; Njimona and Lamparter, 2011).

The first step of photoconversion is a Z to E isomerization of the ring C-D of chromophore (Heyne et al., 2002; van Thor et al., 2007; Andel et al., 1996; Matysik et al., 1995; Wagner et al., 2005; Yang et al., 2007; Essen et al., 2008; Yang et al., 2008). There is also one report that light-induced rotation of the A pyrrole ring but not that of the D ring is the primary motion of the chromophore during photoconversion (Takala et al., 2014).

Although the light-induced structural changes around the chromophore of bacteriophytochromes have been described in molecular detail, the structural basis for signal transmission from the N-terminal to the C-terminal His kinase is still unclear, because until now there were only few reports concerning the structure of full-length Phys In 2014 Vierstra lab reported on the photosensory module of plant phytochrome (Burgie et al., 2014). Six years later (2020) in the same Versrtra group, the structure of both Pr and Pfr was described. This work gave a better insight into photoconversion (Burgie et al., 2020) and Kraskov et al. (2020) pointed out that intramolecular proton transfer triggers phytochromes' structural changes. In one paper (Li et al., 2010), the 13Å full-length structure of Pr state for *Dr*BphP was obtained using single-particle cryoelectron microscopy and negative staining EM, where the N-terminal domain was found to contribute to the dimerization (Li et al., 2010). In another paper, Bellini and Papiz (2012) solved the Pr structure of a bathy type bacterial phytochrome, *Rp*BphP1, from *Rhodopseudomonas palustris*.

Unlike canonical bacterial phytochromes, RpBphP1 does not transmit phosphorelay signals but forms a complex with the transcriptional repressor RpPpsR2 on photoconversion with far-red light (Bellini and Papiz, 2012). The lack of the full-length structure of Pfr state has prevented the understanding of the precise mechanism of how light signal is transmitted from the photosensory module to the histidine kinase module. Apart from this, the authors are also interested in knowing how the histidine kinase activity is activated in BphPs. Marina et al. (2005) first reported on the crystallographic structure of an entire cytoplasmic region of a sensor HK from a thermophilic *Thermotoga maritima*, where the arrangement of the subunits was shown to the be in parallel orientations (Marina et al., 2005). Later, Dago et al. (2012) explored the inactive and signal-activated conformational states of the two catalytic domains of *Bacillus subtilis* sensor histidine kinase KinA, and they proposed that HK was activated by causing localized strain and unwinding at the end of the C-terminal helix of the HisKA domain (Dago et al., 2012). Here it is not sure if similar structural changes occurred in the C-terminal HK domain of Phys with the presence of PCM.

Additionally, the situation became more complicated because one of these phytochromes, Cph1 was crystallized in antiparallel (Essen et al., 2008) while the other was in parallel orientation. More interesting, it has been found that the modulation of histidine kinase in BphPs varied from species to species. For instance, in CpBphP and Agp1, Pr exhibited higher autophosphorylation activity than the Pfr state (Esteban et al., 2005; Karniol and Vierstra, 2003). However, stronger Pfr activity had been reported for Agp2 and *P. syringae* phytochrome (Lamparter et al., 2002; Hubschmann et al., 2001). In contrast, no remarkable difference between Pr and Pfr activity was observed for *Pa*BphP (Tasler et al., 2005). Obviously, it is worth investigating the signal transmission details in different BphPs.

In this work the full-length Agp1 from the soil bacteria *Agrobacterium tumefaciens* is used as a model bacterial phytochrome. Agp1 showed strong His kinase activities in Pr and weak in the Pfr (Karniol and Vierstra, 2003; Lamparter et al., 2002). It was postulated that the structures of the dark-adapted Pr form and red light irradiated Pfr state differed from each other (Noack et al., 2007). In contrast, the authors PELDOR studies on Agp1 gave no major structural difference between Pr and Pfr (Kacprzak et al., 2017).

Therefore, it is necessary to check if there exist some structural differences using other methods. In the present work, mutants were constructed by introducing single accessible Cys at selected positions in the wildtype that is, A362C, K514C, H554C, R603C, I653C, and V674C mutants.

Subsequently, they expressed, purified, and labeled the Cys residue using Atto495 and Atto565 in each mutant, and then detected the fluorescence changes during the photoconversion. It was found that: (1) FRET occurs between Atto495 and Atto565 labels in the subunit of the homodimer labeled protein. This excludes the possibility of antiparallel arrangement of two subunits in Agp1; (2) there are changes in the protein environment as seen by the Pr→ Pfr changes of the monolabeled samples; and (3) different from the major changes predicted from the models, there are only minor changes seen in labeled Agp1.

MATERIALS AND METHODS

Construction of mutants, protein expression, and purification

A series of mutants were constructed using the site-directed mutagenesis method. Six full-length Agp1 mutants A362C, K514C, H554C, R603C, I653C, and V674C are described in this paper. These mutated proteins were expressed in *Escherichia coli* XL1-Blue host cell at 18^{o}C. 50 µM IPTG was added to the cell culture to induce protein expression. The protein both wildtype and the various mutants were purified using Ni^{2+}-NTA affinity column as described previously (Noack et al., 2007).

Protein labeling with fluorescence dye

Unlike the other case, where the protein can be directly labeled using fluorescence dyes, in this work the apoprotein was first assembled with biliverdin (BV) to form the holoprotein prior to the fluorescence labeling. The procedure was described in detail (Njimona, 2012).

The purified apoprotein was dissolved in 50 mM Tris-HCl buffer (pH 7.4, containing 300 mM NaCl and 5 mM EDTA), and the final concentration was ~10 µM (Kacprzak et al., 2017) used ~10:1 of protein to TCEP ratio to reduce the disulphide bond for 30 min at 25°C. The reduced apoprotein was assembled with ~3 times molar excess BV to form the holoprotein. Without removing BV, the holoprotein mixture was incubated in darkness with a 2-fold molar excess of dyes containing 1:1 equal mole of donor Atto495 and acceptor Atto565 for 2 h at 25°C. This reaction was stopped by adding 150-fold molar excess β-mercaptoethanol to react for 30 min. ThTlabeledoteins were separated from free dyes by combining precipitation of 50% ammonium sulfate with NAP-10 desalting column purification process. The purification procedure was repeated two times. As a control, the authors synthesized the single-labeled Agp1 mutants. All the labeled protein was loaded to 15% SDS-PAGE gel. Fluorescence imaging was detected using Safe Imager (Invitrogen Company) prior to protein staining.

Detection of histidine kinase activity

Phosphorylation experiments were carried out under blue-green safelight according to the procedure described in reference (Esteban et al., 2005). The concentration of the wild-type Agp1 or fluorescence-labeled holoprotein was ~0.4 mg/mL based on the absorbance at 703 nm. After 5 µL of each sample was irradiated with 655 nm red light (forming Pfr state) or kept in darkness (forming Pr state), 15 µL phosphorylation buffer containing 25 mM Tris-HCl, 5mM $MgCl_2$, 4 mM mercaptoethanol, 50 mM KCl, 5% ethylene glycerol and 45 µM (50 MBq/mL) [γ-^{32}P] ATP was immediately added to each sample. The mixtures were then incubated at RT for 30 min. The phosphorylation reaction was quenched by addition of 10 µL SDS loading buffer (30% glycerol, 6% SDS, 300 mM DTT, 0.01% bromophenol blue, 240 mM Tris-HCl, pH 6.7).

Subsequently, 10 µL of the sample was loaded to 10% SDS-PAGE gel. Following electrophoresis, the labeled protein was transferred to PVDF membrane using a Trans-Blot semi-dry blot apparatus (Bio-Rad). After the membrane was then exposed to a phosphor-imager plate for about 1h, fluorescent imager analyzer FLA 2000 (Fuji) was used for quantification analysis. In order to see the Coomassie-staining protein bands, the membrane was firstly washed using 100% methanol, and then transferred and kept in water for a short time. Subsequently, the membrane was incubated in Simply Blue safe stain (Invitrogen) followed by shaking in 50% methanol until the protein band appeared. Phosphorylation experiments were also conducted for the holoproteins of six Agp1 mutants under the same condition.

Absorption and fluorescence spectra

Absorption spectra were recorded using on Jasco V-550 spectrometer. For the photoconversion experiment, the sample was irradiated for 2 min using a ~655 nm-emitting LED as described before (Kacprzak et al., 2017). Fluorescence spectra were recorded on Jasco FP-8300 spectrofluorometer. The excitation wavelength was fixed at 470 nm, and the excitation and emission slit widths were 2.5 nm for all the spectra. Because the fluorescence emission spectra of the dyes had a heavy spectral overlapping with the Q band absorption spectrum of biliverdin, when we measured the fluorescence emission spectra, the authors diluted the concentration of the labeled mutants to A_{703} of ~ 0.1 to avoid the inner-filter effect.

RESULTS

Generation of surface cysteine variants

In wild type Agp1 there exist three Cys residues, that is, Cys20, Cys279, and Cys295, in which Cys20 residue is essential for biliverdin binding and photoconversion. In the authors' previous work, they had constructed one full-length Agp1-M8, which contained only Cys20, while the other two Cys279 and Cys295 were mutated to Ala and Ser, respectively. In this work, they created six cysteine single variants of Agp1 based on this mutant M8. Their mutagenesis sites were located close to the beginning of PHY domain (A362C), at the positions between PHY domain and HisKA (K514C, H554C), between HisKA and HATPase (R603C), and in the HATPase domain (I653C, V674C). SDS-PAGE analysis revealed that these mutated proteins were expressed mainly in the soluble form in *E. coli* XL1-Blue host cell, and the resultant supernatant could be purified using Ni^{2+}-NTA column.

Absorption spectra of labeled products

Figure 1A-D showed the UV-vis and NIR absorption spectra of the single-labeled and double-labeled proteins. As a comparison, the absorption spectra of all the holoproteins were also measured. As seen from Figure

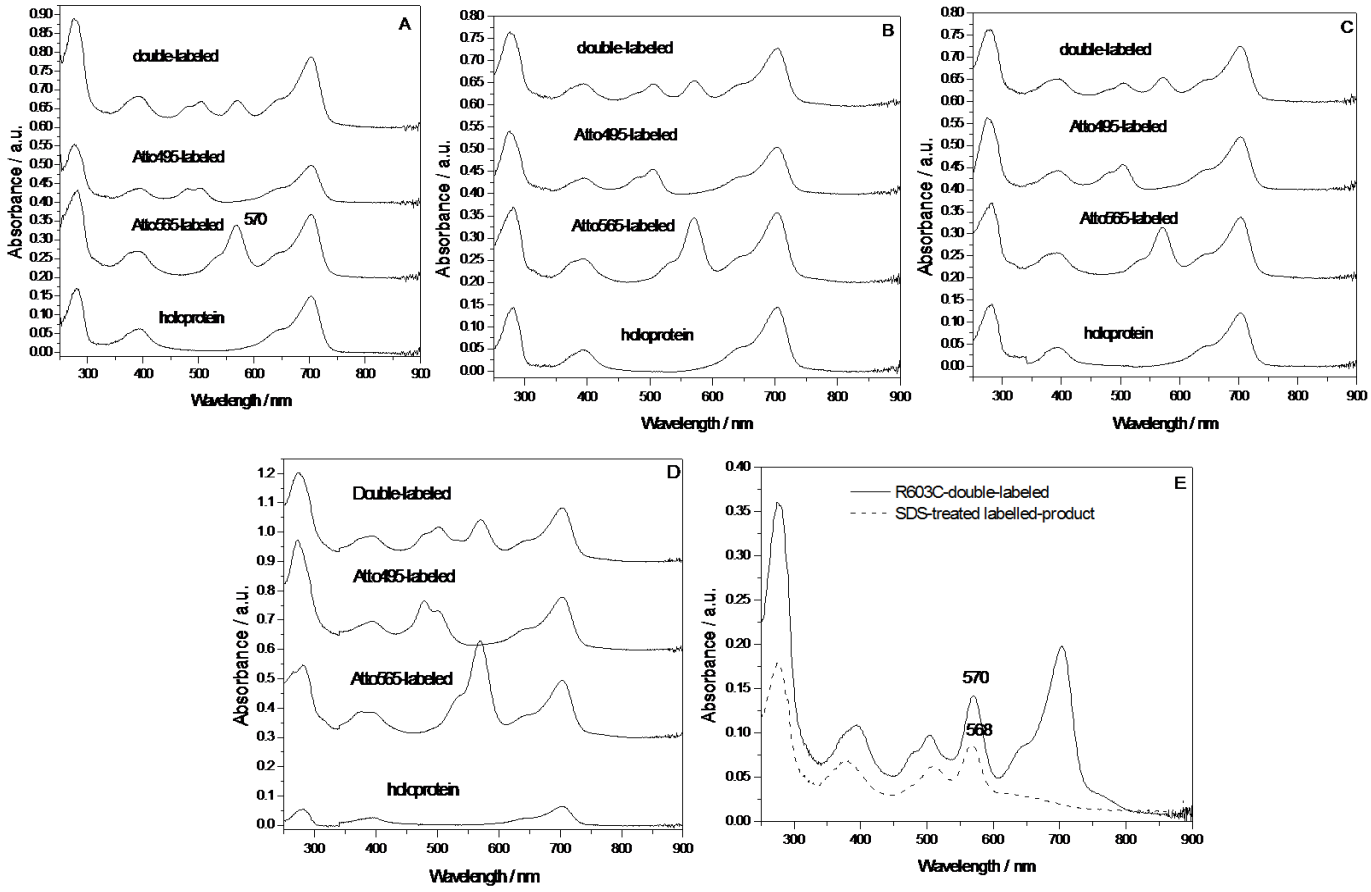

Figure 1. Absorption spectra of holoprotein, single-labeled and double-labeled A326C(A), K517C(B), H554C(C) and R603C(D) in 50 mM Tris-HCl buffer (pH 7.8) containing 300 mM NaCl and 5 mM EDTA after removing the free dyes using NAP-10 column twice, as well as the absorption spectra of double-labeled R603C mutant with and without the treatment of 1% SDS (E).
Source: Author

1A-1D, under the darkness both the labeled samples and the holoproteins exhibited the same strong absorption peak at ~ 704 nm in Pfr state. These results indicated that BV molecules had bcooperated with the apoproteins. As for the Atto dyes it was found that the bound Atto565 in the labeled sample had the maximum absorption peak (λ_{max}) at 570 nm, while the free Atto565 exhibited λ_{max} at 565 nm. Similar spectral red-shift phenomenon was observed for the Atto495 molecule, where the absorption peak shifted from 495 nm (free form) to 505 nm (bounded form). These data suggested that Atto565 molecule and Atto495 molecules had been bound to a more hydrophobic environment. Next, to check if the covalent bond had been formed between Atto dyes and the holoprotein, the authors denatured the labeled holoprotein using 1% SDS, and then used NAP-10 column to remove the free dyes. As seen from Figure 1E, in the collected eluting components the authors still observed the characteristic absorption peaks coming from these two dyes. This phenomenon suggested that there indeed occurred covalent binding between the dyes and the holoprotein.

As demonstrated in Table 2, although maximum fluorescence emission peak λ_{max} experienced no remarkable changes when changing from one mutant to another mutant, full width at half maxima (FWHM) varied from 27 nm (in K517C and in H554C) to 35 nm (A362C) and 41 nm (R603C). The widen spectrum probably reflected the heterogeneous distribution of the donor molecules especially in Agp1-R603C mutant. When the authors further investigated the relative fluorescence quantum yield, we found that the larger the FWHM, the lower the ϕ_f (Table 2).

Although they got some useful information, here they had to consider three possibilities for FRET: 1) FRET occurred between these dyes combined to the mutated Cys residue; 2) FRET occurred between the dyes combined to Cys20; 3) FRET occurred between the dyes combined to the mutated Cys and the dye combined to Cys20 residue in one subunit.

For the first case, the authors can use the mutants which did not contain Cys20, but the mutated Cys was still

Table 1. Photophysical parameters of mono-labeled samples at Pr and Pfr state.

Sample	Absorption peak/nm		Fluorescence peak/nm		FWHM/nm
	Pr	Pfr	Pr	Pfr	
Atto495-A362C	503.9	503.5	527.5	525.3	35.3
Atto565-A362C	568.1	569.3	590.9	590.2	21.9
Atto495-K517C	505.8	505.4	527.3	526.5	27.0
Atto565- K517C	570.0	569.8	590.6	590	20.9
Atto495- K554C	504.4	504.4	528.4	529.0	26.9
Atto565- K554C	570.9	570.9	592.5	592.5	21.2
Atto495- R603C	502.7	502.7	527.0	527.0	44.1
Atto565- R603C	569.8	569.8	592.2	591.2	21.7
Atto495- I654C	504.9	505.5	528.8	527.6	41.6
Atto565- I654C	569.8	569.2	591.4	591.4	22.3
Atto495- V674C	504.3	503.9	530.7	530.0	39.7
Atto565- V674C	568.9	568.9	590.2	589.8	23.1

Source: Author

Table 2. Fluorescence labeling efficiency of various mono-labeled and hetero-labeled mutants.

Sample	Labeling efficiency %	Sample	Labeling efficiency%
Atto495-A362C	34.2	Atto495-R603C	51.3
Atto565-A362C	50.9	Atto495-R603C	-
double- A362C	29.7+19.0	double- R603C	52.7+37.6
Atto495-K517C	29.3	Atto495-I654C	22.9
Atto565-K517C	47.4	Atto565- I654C	36.2
double- K517C	39.5+26.1	double- I654C	25.6+20.2
Atto495-K554C	43.6	Atto495-V674C	48.5
Atto565- K554C	48.8	Atto565- V674C	68.6
double- K554C	26.0+21.9	double- V674C	44.4+48.3

Source: Author

present to check the result. For the second case, they can use M8 that only contain Cys20 to compare the results. Both of these two FRET happened between the two subunits. It is known that hydrophobic interaction played a key role to stable the homodimer, so if the authors added enough SDS, the energy transfer will be dramatically diminished. This was what we observed for K517C mutant (Figure 6C). For the third case, the spectral changes can be checked after the protein has been fully denatured using 8M urea or 6M GnHCl. In other words, if the distance is available, they can still observe FRET under high concentration of SDS. It seems that in A362C mutant this intra-subunit energy transfer happened (Figure 10A, B and C).

In addition, the covalent binding was also confirmed by the fluorescence imaging results in Figure 2, where no matter the single-labeled or the double-labeled proteins could emit strong fluorescence after these proteins were separated by SDS-PAGE (seen in lanes 6-8 of Figure 2). Subsequently, the authors roughly calculated the labeling efficiency. Next, the authors calculated the fluorescence labeling efficiency based on the equation:

$$\mathrm{CE} = \frac{\epsilon_{280}(\mathrm{Protein}) \cdot A_{\max}}{(A_{280} - \mathrm{CF}_{280} \cdot A_{\max}) \cdot \epsilon_{\mathrm{dye}}}$$

From the data listed in Table 1, it was realized that the double labeling efficiency of both R603C and V674C reached beyond 85%. K517C mutant had double-labeling efficiency of ~65%. In contrast, the double-labeling efficiency was less than ~50% in the case of A362C, K554C, and I653C. Meanwhile, we observed that although for all mono-labeled mutants, the acceptor Atto565 exhibited higher reactivity than the donor Atto495 did, double-labeled samples contained more dodonors

Fluorescence-labeled protein activity assay

To test whether the fluorescence labeling exert some

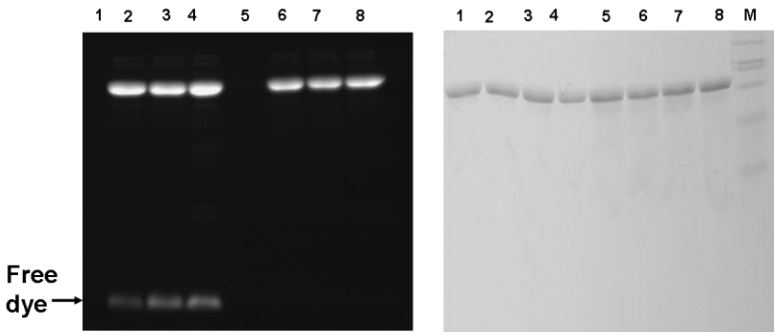

Figure 2. Fluorescence imaging (left) and protein staining result (right) of the labeled holoprotein Agp1-R603C-BV directly quenched by β–mercaptoethanol (lane1-4), purified using NAP-10 column for one time (lane 5-8), respectively. Lane 1 and 5 represent the holoprotein without the dyes. Lanes 2 and 6 represent single-labeled Agp1-R603C using two times of Atto-565. Lane 3 and 7 represent single-labeled Agp1-R603C using two times of Atto-495. Lane 4 and 8 represent double-labeled Agp1-R603C using 1 time of Atto-565 and 1 time of Atto-495, respectively.
Source: Author

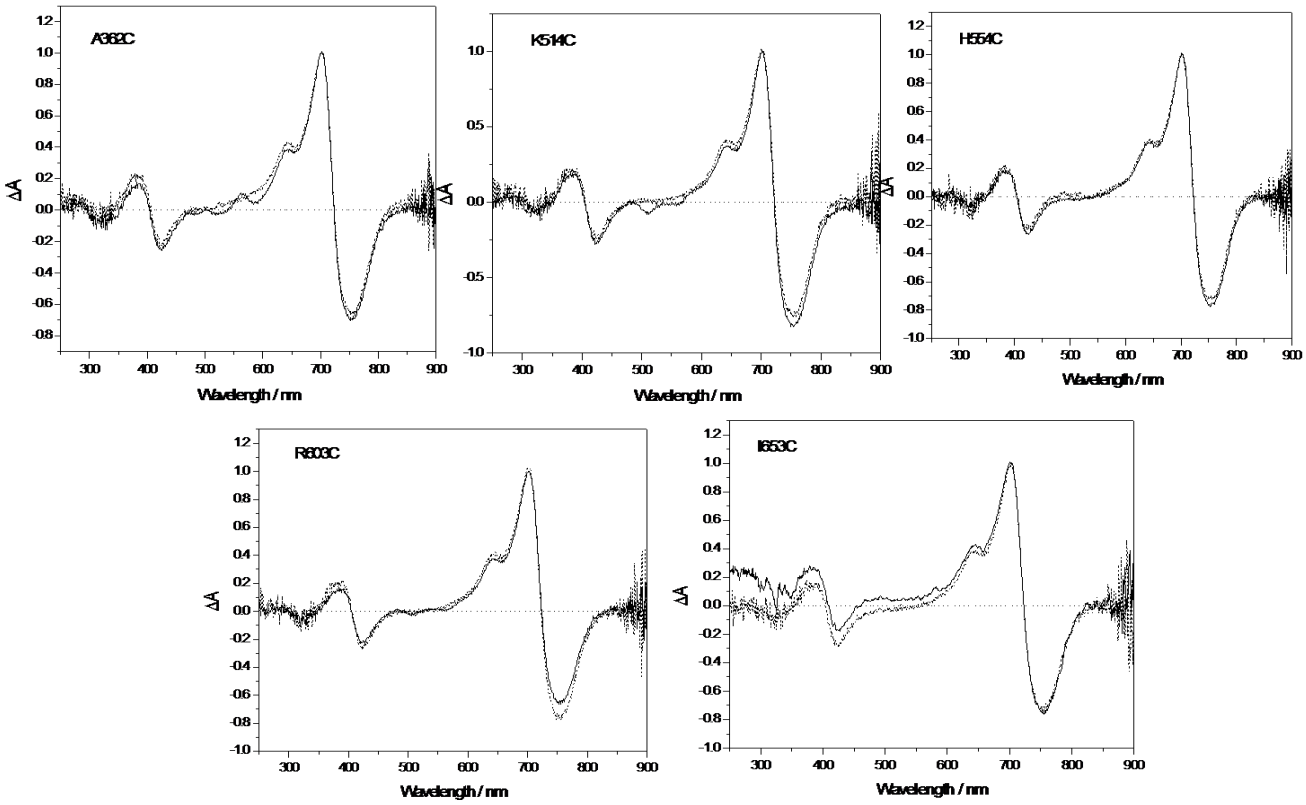

Figure 3. Comparison of difference absorption spectra between Pr and Pfr of double-labeled Agp1 mutants (solid line) and holoproteins (dashed line).
Source: Author

holoprotein and labeled protein. As shown in Figure 3, no significant changes were observed for the maximum absorbance peak of Pr or Pfr. Meanwhile, the absorbance ratio between Pr and Pfr band of the difference spectra experienced only slight changes when Agp1 holoproteins were combined with the dyes. It indicated that the

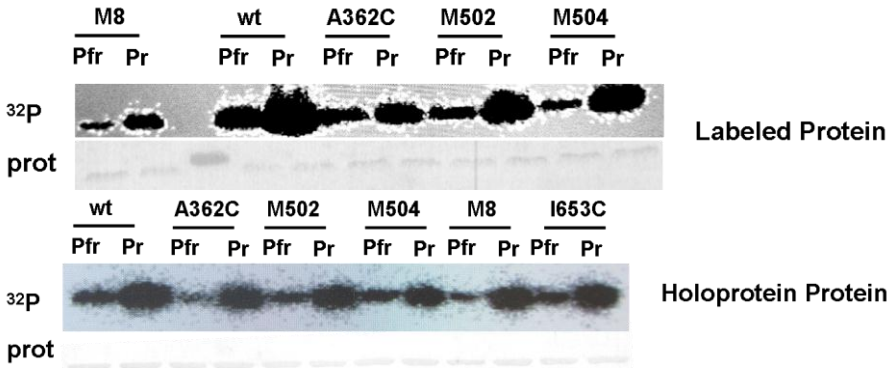

Figure 4. Autoradiogram (above) and Commassie-stained blot (below) of Agp1, double-labeled mutants as well as holoproteins incubated with γ-^{32}P ATP at room temperature.
Source: Author

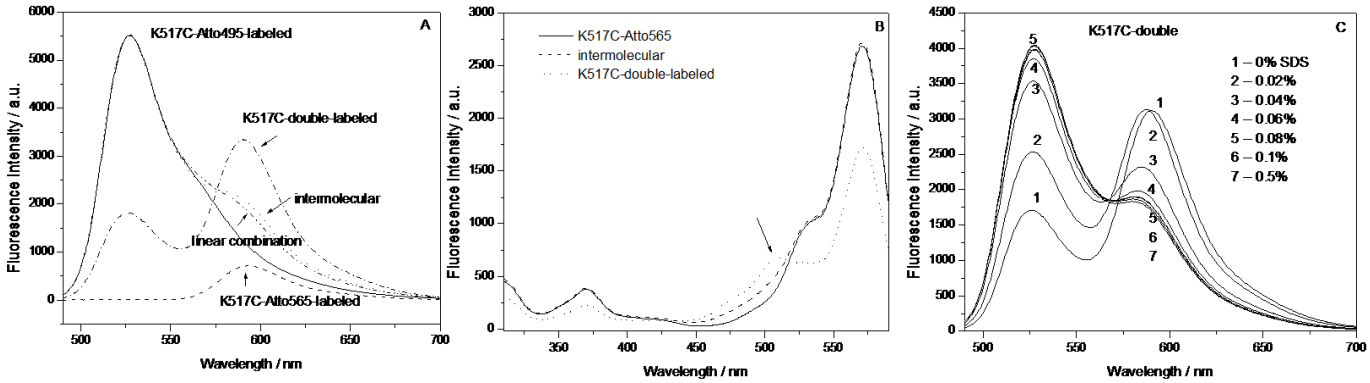

Figure 5. Fluorescence emission spectra of fluorescence-labeled K517C product upon excitation at 470 nm (A), fluorescence excitation spectra of K517C-labeled product with the detection wavelength at 600 nm (B), and the effect of SDS on the fluorescence emission spectra of double-labeled K517C mutant (C) at room temperature.
Source: Author

photochemical activity of various Agp1 mutants is not influenced by the fluorescence dyes. The autophosphorylation activity assay in Figure 4, shows a similar pattern for both the wt Agp1 and the mutants. This demonstrated that the double-labeled Agp1 mutants can act as a light-regulated histidine kinase.

Fluorescence spectra of labeled proteins

Evidence for FRET in the double-labeled homodimer

As shown in Figure 5A, in Atto495-labeled K517C mutant the authors detected one wide and asymmetrical fluorescence emission peak extending from 500 nm to 700 nm following the 470 nm-excitation. Obviously, this peak originated from the donor molecule Atto495. As far as the acceptor molecule was concerned, in principle, it was expected that the acceptor would not be excited simultaneously when they excited the donor. However, in this work, the authors found that the excitation at 470 nm gave rise to one weak fluorescence emission peak at 591 nm (dashed line in Figure 5A), which was assigned to the Atto565 molecule. When the Atto495-labeled was mixed and the Atto565-labeled K517C mutant, the resultant fluorescence emission spectrum is almost identical to their linear combination, where one weak shoulder peak was observed from the Atto565 molecule. In contrast, in the double-labeled K517C mutant, the acceptor exhibits higher fluorescence intensity than the donor. Similar phenomena were observed for the other double-labeled mutants Fluorescence excitation spectra provided another evidence for FRET, where apart from the peak at 370 nm and the 570 nm, the absorbance at 500 nm made some contribution to the emission of the acceptor at 600 nm (the arrow shown in Figure 5B), indicating that the excited donor molecule could transfer the excitation energy to the acceptor (dotted line in Figure 5B). It was not the case for

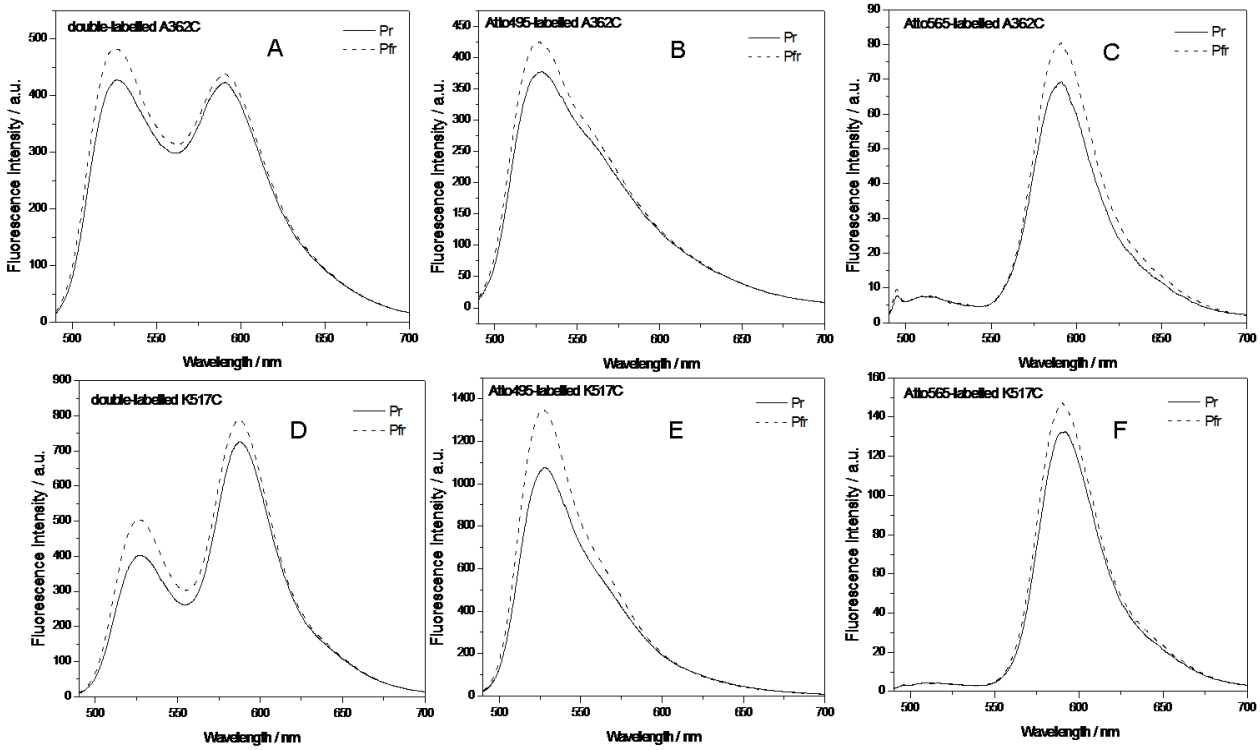

Figure 6. Fluorescence emission spectra of double-labeled, Atto495-labeled and Atto565-labeled A362C mutant (A, B, C) and K517C mutant (D, E, F) upon excitation at 470 nm at RT in the darkness (Pr state, solid line) and after red light irradiation for 2min (Pfr state, dashed line).
Source: Author

the Atto565-labeled and the intermolecular system. In addition, another piece of evidence to support FRET is the effect of SDS on the fluorescence emission spectra. As demonstrated in Figure 5C, the treatment of SDS gave rise to the decrease in fluorescence intensity of the acceptor, meanwhile, the fluorescence intensity of the donor recovered gradually with increasing the concentration of SDS. It suggested that the FRET phenomenon disappeared in a double-labeled K517C mutant with the presence of SDS. The fact that FRET happened in the double-labeled full-length Agp1 mutant helped to exclude the possibility that two subunits in Agp1 were arranged in the antiparallel form.

Fluorescence emission spectral changes during the photoconversion

Figure 6A presented the fluorescence emission spectra of double-labeled A362C in the darkness (solid line) and after 2min-red light irradiation (dashed line) upon excitation at 470 nm. Obviously, the photoconversion from Pr to Pfr leads to an increase in the fluorescence intensity of both the donor and the acceptor. As a control, the authors also measured the spectral changes of the single-labeled sample under the same condition. As seen in Fig. 5B and 5C, no matter for the donor or the acceptor, their fluorescence emission intensity was enhanced upon illumination. Similar changes were observed for the K517C mutant (Figure 6D-F). Different from A362C and K517C mutant, however, no significant spectral changes were detected for the double-labeled H554C (Figure 7A) and double-labeled R603C (Figure 7D) upon red light illumination. When the single-labeled sample was detected, the authors observed similar results (Figure 7B-C and 7D-E). The same phenomenon was detected from I653C and V674C mutants, as described in Figure 8.

DISCUSSION

No full-length BphP structural information has been available for both Pr and Pfr mainly because it was rather difficult to get the high-quality 3D crystals of both Pr and Pfr state simultaneously. Therefore, some indirect spectroscopic methods are currently method of choice to understand these structures. In the previous work, the authors had to use MTSSL nitro oxide spin probe to label single Cys residue in various Agp1 mutants, and then measured dipole-dipole coupling using double electron electron resonance (DEER) technology. This method helped to determine the distance within 5-80 Å between

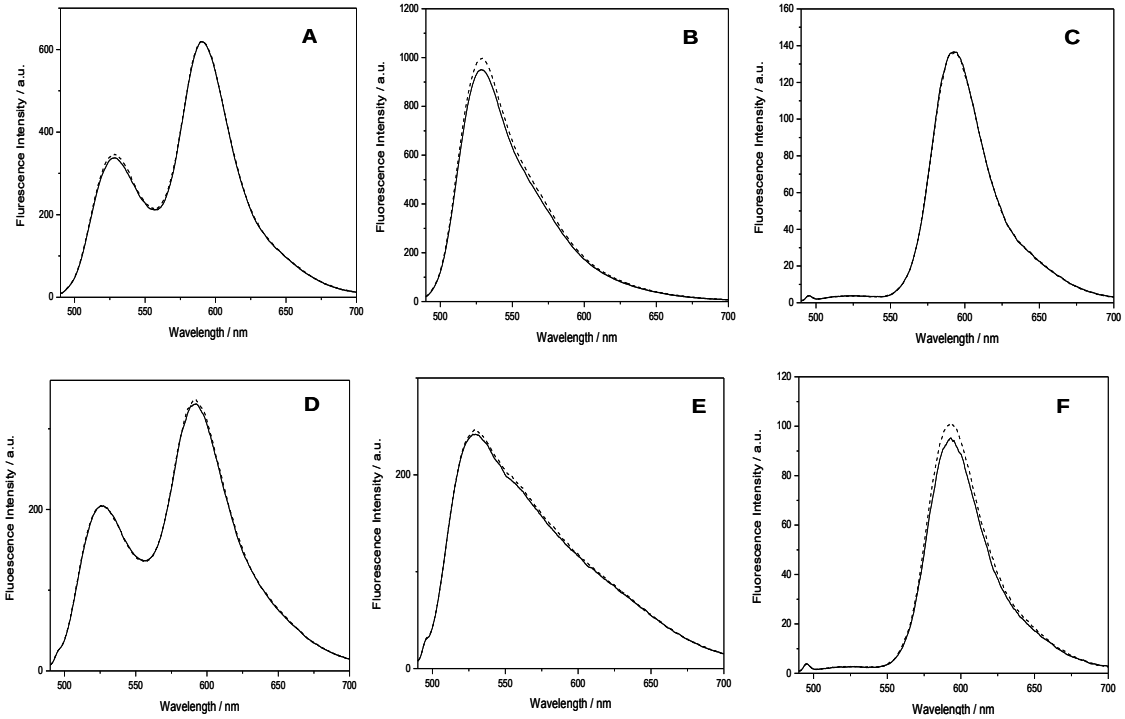

Figure 7. Fluorescence emission spectra of double-labeled, Atto495-labeled and Atto565-labeled H554C mutant (A, B, C) and R603C mutant (D, E, F) upon excitation at 470 nm at RT in the darkness (Pr state, solid line) and after red light irradiation for 2min (Pfr state, dashed line).
Source: Author

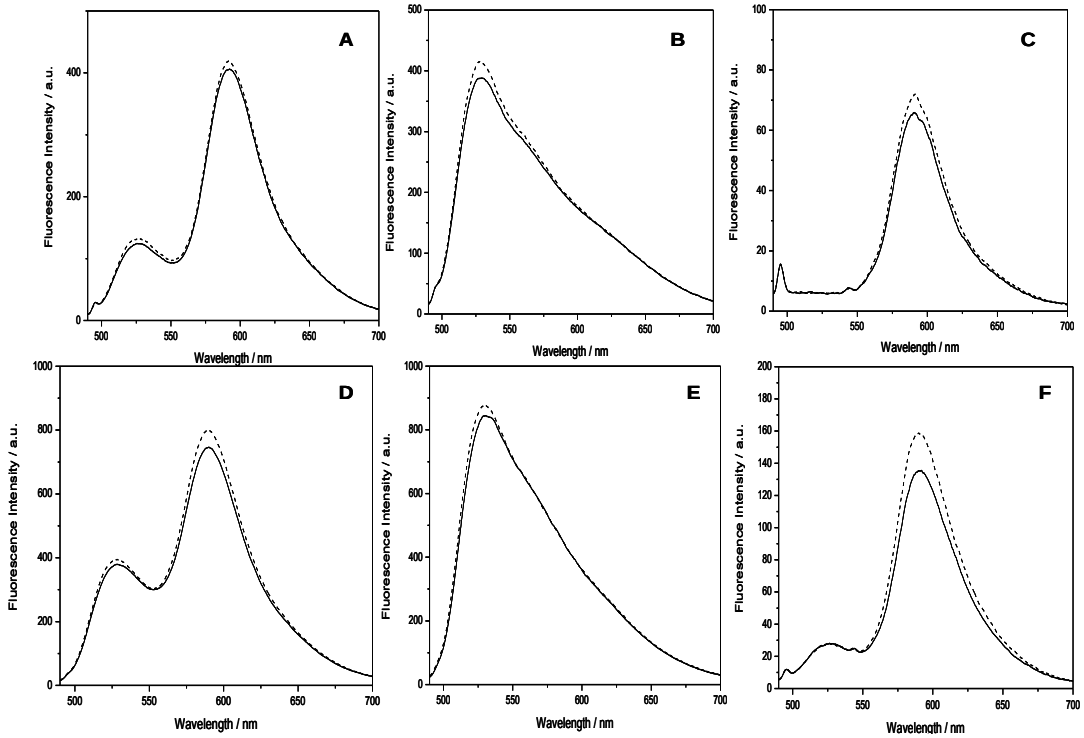

Figure 8. Fluorescence emission spectra of double-labeled, Atto495-labeled and Atto565-labeled I653C mutant (A, B, C) and V674C mutant (D, E, F) upon excitation at 470 nm at RT in the darkness (Pr state, solid line) and after red light irradiation for 2min (Pfr state, dashed line).
Source: Author

two paramagnetic centers. The results showed that no major structural changes happened during the photoconversion of Agp1 mutant (Noack et al., 2007). Different from that case, in this paper we haveused another spectroscopic method, that is, FRET to get some structural information induced by light irradiation. FRET method has been used to investigate dimerization and inter-chromophore distance of Cph1 phytochrome from *Synechocystis*, where the BV analogue PEB and the natural chromophore PCB were used as FRET donor and acceptor, respectively. Both of them were combined to the chromophore-binding site (Otto et al., 2003). Different from their case, in this paper we aimed at employing FRET method to explore the structural changes happening in different domains of full-length Agp1 during the photoconversion, including PAS, GAF, PHY and histidine kinase domain.

Suitable FRET pairs were selected for these measurements. Firstly, taking into consideration that the maleimide function group had high reactivity with thiol groups, site-directed mutagenesis method was used to produce A362C, K514C, H554C, R603C, I653C and V674C mutants as described above. Secondly, because BV itself exhibited one strong absorption peak in 600-750 nm and one weak peak in 350 - 450 nm, in order to avoid the inner filter effect or the competition absorption from BV, Atto495 maleimide and Atto565 maleimide dyes was used as FRET pairs, whose absorption peaks were located in the 400-600 nm range and did not heavily overlap with the absorption peaks of BV.

Thirdly, it was known that the FRET energy transfer efficiency is strongly dependent on the distance between dye pair as well as the FÖrster radius Ro, therefore we roughly calculated the FÖrster radius Ro = ~57.9 Å between Atto495 donor and Atto565 acceptor. According to the reference (Kim et al., 2008), FRET method could provide reliable distance results only when the intermolecular distance between FRET pairs varied from 0.5 R_0 - 1.5 R_0 with the energy transfer efficiency of 8 - 98%. Therefore, it means that in our case, we could investigate the inter-subunits distance changes happening within 29Å – 87Å. Take A362C as an example. X-ray crystallographic data revealed that the inter-subunit distance is nearly ~ 39.5 Å and 45.9 Å for Pr state for Pfr, respectively. Within this range FRET is available to provide the distance information.

This phenomenon suggested that BV molecules had been incorporated with the apoprotein (solid line). Subsequently, the absorbance at ~703 nm decreased immediately following the addition of two times molar excess of Atto495 (Figure 9B), Atto565 (Figure 9C), or their 1:1 mixture (Figure 9D) to initiate the labeling experiments, respectively. A similar phenomenon was observed when we only added the same amount of DMSO solvent that had been used to dissolve the dyes (Figure 9B). It indicated that the decrease of A_{703} might be due to the fast micro-environmental changes of the BV-binding pocket induced by solvent. During the subsequent 2h labeling reactions, $A_{703\ nm}$ experienced no remarkable changes were seen in Figure 9A to D. It inferred that the presence of 2-fold of the dyes would not lead to the displacement of BV molecules by FRET pairs away from the binding site. It seemed reasonable because Cys20 was located in the hydrophobic chromophore-binding pocket, and therefore it could not be easily attacked by the FRET pairs.

The fluorescence labeling efficiency was also analyzed as shown in Table1, and found that FRET pairs exhibited different reactivity against Cys residues located in different domains. The protein sample contains a mixture of unlabeled holoprotein (00) and labeled holoprotein (AA or DD). In contrast, there coexisted AA, DD, AD, DA as well as non-labeled samples in the double-labeled mutants. In the latter work, although we paid more attention to the double-labeled samples, as a control, we also performed the same experiment on the single-labeled samples.

Next, it was necessary to test if the fluorescence labeling would affect the photoconversion behavior or biological activity of Agp1 mutants. As shown in Figure 3, the light-induced difference absorption spectral data revealed that the photochemical activity of various Agp1 holoproteins was not influenced by the external FRET pairs. As for the biological activity, the authors detected the histidine kinase activity by using γ-^{32}P ATP. It was found from Figure 4 that in the labeled sample, Pr displayed stronger autophosphorylation activity than Pfr form. This result was almost identical to the wt Agp1.

Following the biological activity assay, the static fluorescence spectroscopic method was used to check the fluorescence emission of double-labeled mutants. By comparing the intermolecular and intramolecular fluorescence emission spectra, as well as the fluorescence excitation spectra, we concluded that as we had expected, the fluorescence resonance energy transfer happened from the Atto495 to Atto565 in all mutants this confirms parallel orientation of dimeric Agp1 subunits.

The authors tried to get some information from the spectra of monolabeled samples. As demonstrated in Table 1, Atto495-labeled R603C exhibited the maximum FWHM of ~44 nm among all samples; meanwhile Atto495-labeled A362C much displayed larger FWHM than other mutants. It suggested that there might co-exist heterogeneous distribution of Atto495 molecules in Atto495-labeled R603C and A362C most probably resulting from the larger flexibility in such domains. However, it was surprising that no similar results were observed for Atto565-labeled samples As shown in Figure 6B and 6E, the conversion from Pfr to Pr led to a remarkable increase in fluorescence intensity at 572 nm in both Atto495 labelled A326C mutant and Atto495 labelled H517C mutant. In contrast, no significant changes were observed for Atto495 labelled H554C,

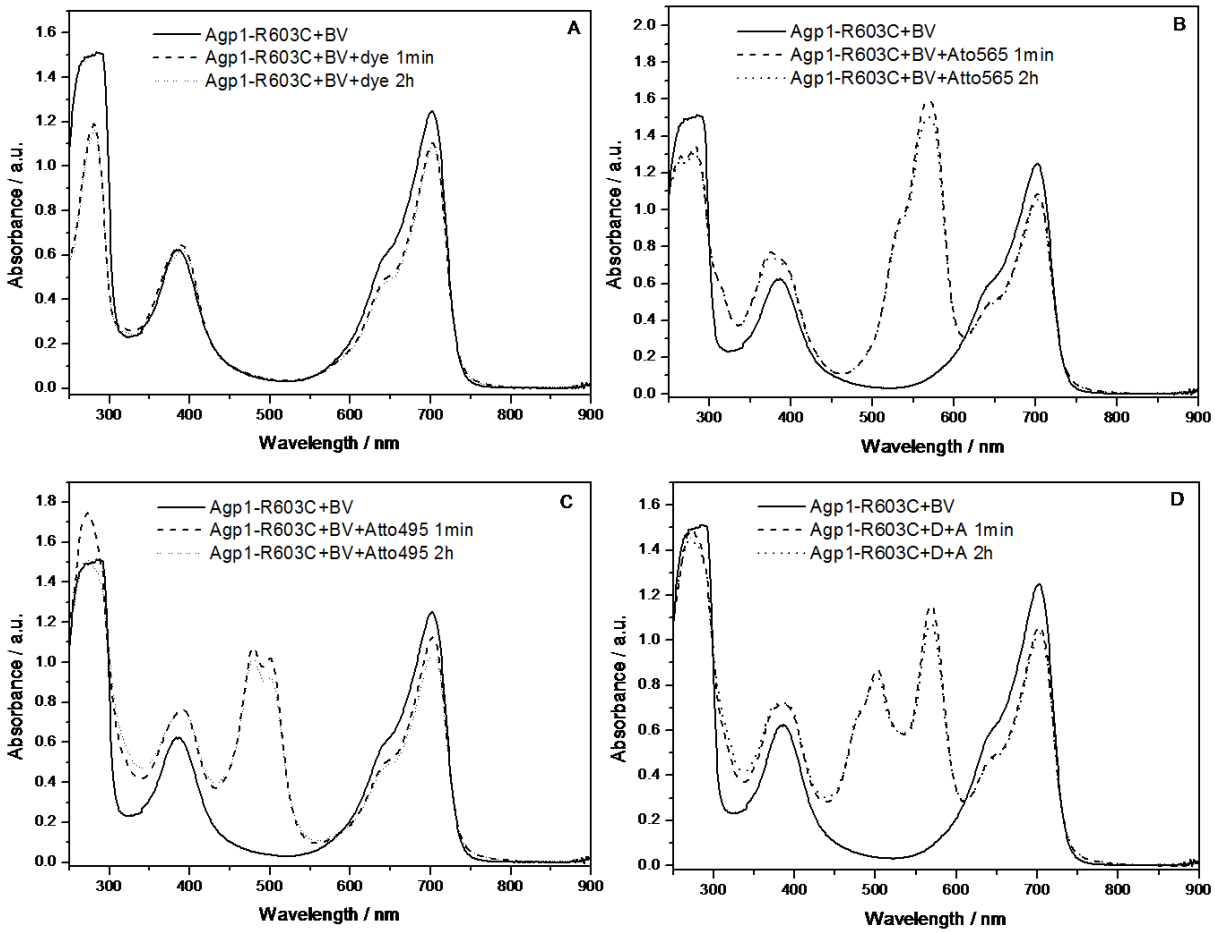

Figure 9. Uv-Vis NIR absorption spectra of Agp1-R603C holoproten incubated with DMSO (A), 2 times fold of Atto565 (B), 2 times fold of Atto495 (C), 1 time of Atto495 and 1 time of Atto565 (D) during the fluorescence labeling process.
Source: Author

Atto495 LABELED R603C as well as Atto495 labelled I653C and V674Cc. There are changes in the protein environment as seen by the Pr→ Pfr changes of the monolabeled samples. Different from the major changes predicted from the models, there are no or minor changes.

In a summary the authors found that: (1) FRET efficiency changed from one position to another position. When they compared A362C, K517C, and H554C, they observed that in K517C energy transfer efficiency was the highest. According to the crystallographic data, the distance at site 517 between two subunits was nearly 40 nm, and (2) in comparison with Pr, Pfr form displayed higher energy transfer efficiency. It is inferred that the distance would become shorter in the Pfr state. As for the R603C mutant, this method could not be used because its donor exhibited some unusual spectral behavior.

Conclusion

Although the labeling strategy is simpler for DEER technology because only one kind of interacting labels is needed while FRET pairs are required, the authors can obtain some orientation information by measuring the fluorescence polarization or anisotropy in FRET measurement. As described in the introduction, PHY domain experienced some variations during the photoconversion, so they constructed one mutant targeting PHY domain. Additionally, they suspected that like the other histidine kinase, some changes happened in His KA and ATPmase domain. We mainly focused on PHY, helix, ATPmase domain and could identify some of these changes.

ACKNOWLEDGEMENT

Special thanks to the laboratories of Prof. Tilman Lamparter and Ann Ulrich in Karlsruhe Institute of Science and Technology in which some of the experiments were performed. We also thank center for international migration (CIM) in GIZ for partial financial support.

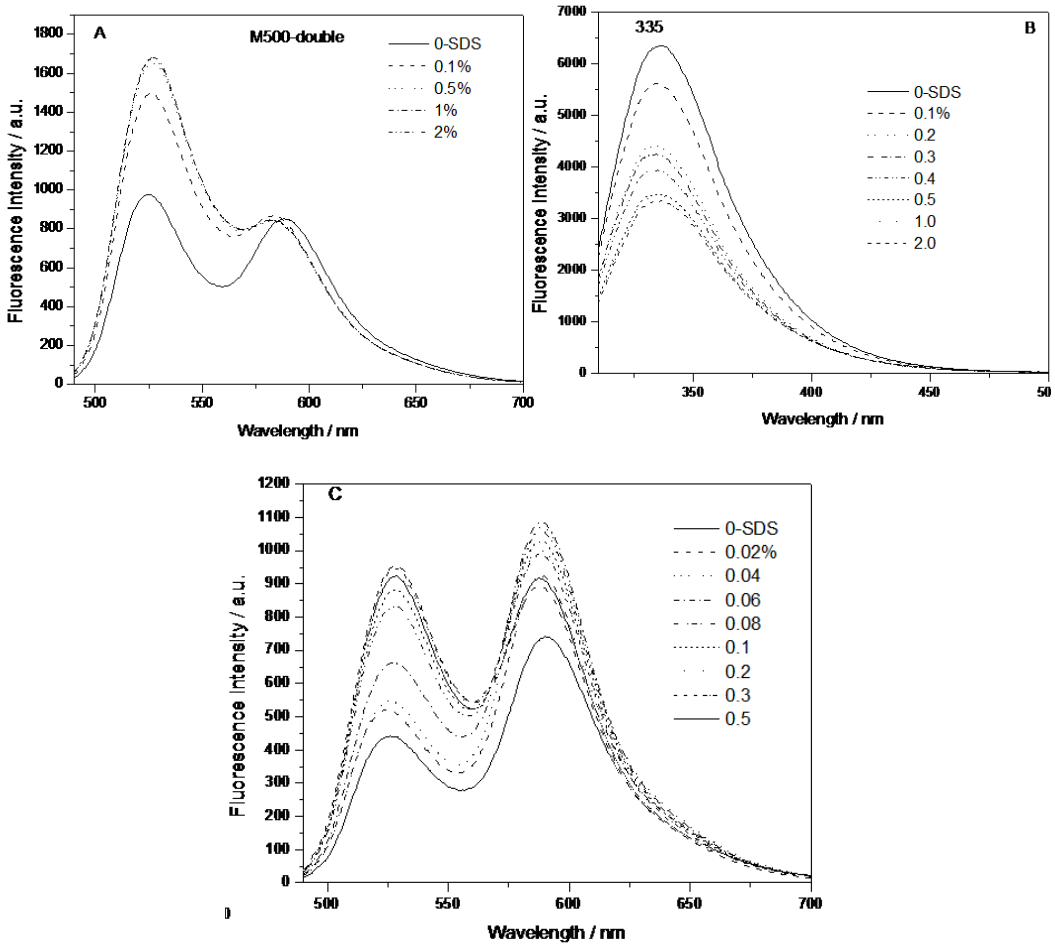

Figure 10. The effect of SDS on the fluorescence emission spectra of double-labeled M500 upon excitation at 470 nm (A), the intrinsic fluorescence following the excitation at 290 nm (B) and the fluorescence emission spectra of double-labeled A362C mutant (C).
Source: Author

CONFLICT OF INTERESTS

The authors have not declared any conflicts of interests.

REFERENCES

Andel F, Lagarias JC, Mathies RA (1996). Resonance raman analysis of chromophore structure in the lumi-R photoproduct of phytochrome. Biochemistry 35(50):15997-16008.

Barkovits K, Schubert B, Heine S, Scheer M, Frankenberg-Dinkel N (2011). Function of the bacteriophytochrome BphP in the RpoS/Las quorum-sensing network of *Pseudomonas aeruginosa*. Microbilogoy 157(6):1651-1664.

Bellini D, Papiz MZ (2012). Structure of a bacteriophytochrome and light-stimulated protomer swapping with a gene repressor. Structure 20(8):1436-1446.

Bhoo SH, Davis SJ, Walker J, Karniol B, Vierstra RD (2001). Bacteriophytochromes are photochromic histidine kinases using a biliverdin chromophore. Nature 414(6865):776-779.

Burgie ES, Bussell AN, Walker JM, Dubiel K, Vierstra RD (2014). Crystal structure of the photosensing module from a red/far-red light-absorbing plant phytochrome. Proceedings of the National Academy of Sciences 111(28):10179-10184

Burgie ES, Clinger JA, Miller MD, Brewster AS, Aller P, Butryn A, Fuller FD, Gul S, Young ID, Pham CC, Kim IS (2020). Photoreversible interconversion of a phytochrome photosensory module in the crystalline state. Proceedings of the National Academy of Sciences 117(1):300-307.

Dago AE, Schug A, Procaccini A, Hoch JA, Weigt M, Szurmant H (2012). Structural basis of histidine kinase autophosphorylation deduced by integrating genomics, molecular dynamics, and mutagenesis. Proceedings of the National Academy of Sciences 109(26):E1733-1742

Davis SJ, Veneer AV, Vierstra RD (1999). Bacteriophytochromes: Phytochrome-like photoreceptors from nonphotosynthetic eubacteria. Science 286:2517-2520.

Essen LO, Mailliet J, Hughes J (2008). The structure of a complete phytochrome sensory module in the Pr ground state. Proceedings of the National Academy of Sciences 105(38):14709-14714.

Esteban B, Carrascal M, Abian J, Lamparter T (2005). Light-induced conformational changes of cyanobacterial phytochrome Cph1 probed by limited proteolysis and autophosphorylation. Biochemistry 44(2):450-461.

Fixen KR, Baker AW, Stojkovic EA, Beatty JT, Harwood CS (2014). Apo-bacteriophytochromes modulate bacterial photosynthesis in response to low light. Proceedings of the National Academy of

Sciences 111(2):237-244
Giraud E, Fardoux J, Fourrier N, Hannibal L, Genty B, Bouyer P, Dreyfus B, Verméglio A (2002). Bacteriophytochrome controls photosystem synthesis in anoxygenic bacteria. Nature 417(6885):202-205.
Giraud E, Verméglio A (2008). Bacteriophytochromes in anoxygenic photosynthetic bacteria. Photosynthesis Research 97(2):141-153.
Giraud E, Verméglio A (2012). Isolation and Light-Stimulated Expression of Canthaxanthin and Spirilloxanthin Biosynthesis Genes from the Photosynthetic Bacterium Bradyrhizobium sp. Strain ORS278. InMicrobial Carotenoids from Bacteria and Microalgae 2012 (pp. 173-183). Humana Press, Totowa, NJ.
Heyne K, Herbst J, Stehlik D, Esteban B, Lamparter T, Hughes J, Diller R (2002). Ultrafast dynamics of phytochrome from the cyanobacterium synechocystis, reconstituted with phycocyanobilin and phycoerythrobilin. Biophysical Journal 82(2):1004-1016.
Hubschmann T, Jorissen HJ, Bo¨rner T, Gartner W, Tandeau de Marsac N (2001). Phosphorylation of proteins in the light-dependent signalling pathway of a filamentous cyanobacterium. European Journal of Biochemistry 268:3383-3389.
Kacprzak S, Njimona I, Renz A, Feng J, Reijerse E, Lubitz W, Krauss N, Scheerer P, Nagano S, Lamparter T, Weber S. Intersubunit distances in full-length, dimeric, bacterial phytochrome Agp1, as measured by pulsed electron-electron double resonance (PELDOR) between different spin label positions, remain unchanged upon photoconversion. Journal of Biological Chemistry 292(18):7598-7606.
Karniol B, Vierstra RD (2003). The pair of bacteriophytochrome from *Agrobacterium tumefaciens* are histidine kinases with opposing photobiological properties. Proceedings of the National Academy of Sciences 100:2807-2812
Kim Y, Ho SO, Gassman NR, Korlann Y, Landorf EV, Collart FR, Weiss S. Efficient site-specific labeling of proteins via cysteines. Bioconjugate Chemistry 19(3):786-791.
Kraskov A, Nguyen AD, Goerling J, Buhrke D, Velazquez Escobar F, Fernandez Lopez M, Michael N, Sauthof L, Schmidt A, Piwowarski P, Yang Y, Stensitzki T, Adam S, Bartl F, Schapiro I, Heyne K, Siebert F, Scheerer P, Mroginski MA, Hildebrandt P (2020). Intramolecular proton transfer controls protein structural changes in phytochrome. Biochemistry 59(9):1023-1037.
Lamparter T, Michael N, Mittmann F, Esteban B (2002). Phytochrome from Agrobacterium tumefaciens has unusual spectral properties and reveals an N-terminal chromophore attachment site. Proceedings of the National Academy of Sciences 99(18):11628-11633.
Li H, Zhang J, Vierstra RD, Li H (2010). Quaternary organization of a phytochrome dimer as revealed by cryoelectron microscopy. Proceedings of the National Academy of Sciences 107(24):10872-10877.
Marina A, Waldburger CD, Hendrickson WA (2005). Structure of the entire cytoplasmic portion of a sensor histidine-kinase protein. EMBO Journal 24(24):4247-4259.
Matysik J, Hildebrandt P, Schlamann W, Braslavsky SE, Schaffner K (1995). Fourier-transform resonance Raman spectroscopy of intermediates of the phytochrome photocycle. Biochemistry 34(33):10497-10507.
Njimona I (2012). Molecular Studies on Light-induced Protein Conformational Changes on Agrobacterium Tumefaciens Phytochrome, Agp1. Mensch und Buch.
Njimona I, Lamparter T (2011). Temperature effects on Agrobacterium phytochrome Agp1. Plos ONE 6(10):e25977
Noack S, Michael N, Rosen R, Lamparter T (2007). Protein conformational changes of Agrobacterium phytochrome Agp1 during chromophore assembly and photoconversion. Biochemistry 46(13):4146-4176.
Otto H, Lamparter T, Borucki B, Hughes J, Heyn MP (2003). Dimerization and inter-chromophore distance of Cph1 phytochrome from *Synechocystis*, as monitored by fluorescence homo and hetero energy transfer. Biochemistry 42(19):5885-5895
Takala H, Björling A, Berntsson O, Lehtivuori H, Niebling S, Hoernke M, Kosheleva I, Henning R, Menzel A, Ihalainen JA, Westenhoff S (2014). Signal amplification and transduction in phytochrome photosensors. Nature 509(7499):245-248.
Tasler R, Moises T, Frankenberg-Dinkel N (2005). Biochemical and spectroscopic characterization of the bacterial phytochrome of Pseudomonas aeruginosa. FEBS Journal 272(8):1927-1936.
van Thor JJ, Ronayne KL, Towrie M (2007). Formation of the early photoproduct lumi-R of cyanobacterial phytochrome cph1 observed by ultrafast mid-infrared spectroscopy. Journal of the American Chemical Society 129(1):126-132.
Wagner JR, Brunzelle JS, Forest KT, Vierstra RD (2005). A light-sensing knot revealed by the structure of the chromophore-binding domain of phytochrome. Nature 438(7066):325-331.
Yang X, Kuk J, Moffat K (2008). Crystal structure of *Pseudomonas aeruginosa* bacteriophytochrome: photoconversion and signal transduction. Proceedings of the National Academy of Sciences 105(38):14715-14720.
Yang X, Stojković EA, Kuk J, Moffat K (2007). Crystal structure of the chromophore binding domain of an unusual bacteriophytochrome, RpBphP3, reveals residues that modulate photoconversion. Proceedings of the National Academy of Sciences 104(30):12571-12576.
Yeh KC, Wu SH, Murphy JT, Lagarias JC (1997). A cyanobacterial phytochrome two-component light sensory system. Science 277(5331):1505-1508.

Vol. 12(2) pp. 22-30, July-December 2022
DOI: 10.5897/IJBMBR2022.0330
Article Number:1AC99CB69664
ISSN 2141-2154
Copyright © 2022
Author(s) retain the copyright of this article
http:// www.academicjournals.org/IJBMBR

ACADEMIC JOURNALS
expand your knowledge

International Journal of Biotechnology and Molecular Biology Research

Full Length Research Paper

Root and hypocotyl growth of *Arabidopsis* seedlings grown under different light conditions and influence of TOR kinase inhibitor AZD

Xingyu Yan[1], Felipe Yamashita[1], Njimona Ibrahim[2,3]* and Baluška František[1]

[1]Institute of Cellular and Molecular Botanics (IZMB), University of Bonn, Bonn, Germany.
[2]Institute of Medical Research and Medicinal Plants Studies (IMPM), Ministry of Scientific Research and Innovation, Yaoundé, Cameroon.
[3]Bamenda University of Science and Technology (BUST), Bamenda, Cameroon.

Received 1 July, 2022; Accepted August 18, 2022

We set up six light conditions to investigate the changes in the development of *Arabidopsis thaliana* hypocotyls and roots. Seedlings grown for 96 h under darkness were scored with shorter roots and longer hypocotyls. In shoot-shaded conditions, seedlings were unable to carry out photosynthesis, resulting in insufficient stored nutrients for root development. In the three groups of different light intensities applied to the roots, total light caused stress in the entire seedlings and the length of roots and hypocotyls were shorter than in conditions when roots were growing within light-dark gradients. Importantly, root lengths were higher within light-dark gradients than in total light. Different light treatments did significantly affect root growth and hypocotyl growth. The addition of ATP-competitive mTOR kinase inhibitor (AZD), drastically reduced root, however, this did not occur with hypocotyl length.

Key words: Total light, total dark, gradient light, shoot dark with light blocker, light blocker, shoot dark.

INTRODUCTION

To adapt to a changing environment, all living organisms have to respond appropriately to circumstances. Unlike animals, plants are unable to move away from extremes in their surrounding environment or move towards a nutrition source. However, plants have a flexible pattern of development that allows them to adjust their organ number and size (architecture) to the changing environment. The fundamental body plan of the mature plant is generated during the early stages of embryogenesis (Jürgens et al., 1991). This process involves the production of shoot and root meristem, cotyledons, radicle and hypocotyls.

In animals, most organs are already present by the time the embryo is fully formed. On the contrary, most organs in plants are formed after embryogenesis is finished. Once dormancy is broken, the seeds begin to

*Corresponding author. E-mail: njimona@yahoo.com.

Author(s) agree that this article remain permanently open access under the terms of the Creative Commons Attribution License 4.0 International License

germinate with the formation of primary plant organs: roots, shoots, and leaves (Kadereit et al., 2014). Roots emerge from root meristems located at the tip of the root, while the aboveground shoot system generates from shoot meristems (Brand et al., 2001). Roots are the underground part of the plant body that is required for anchorage in the substrate, uptake of water and ion, and synthesis of phytohormones (Kadereit et al., 2014). The root apex also has an oscillatory zone (Baluška and Mancuso, 2013). The root apex is subdivided into four zones: Meristematic (Kadereit et al., 2014), transition (Verbelen et al., 2006, Baluška et al., 2010), elongation, and differentiation zones. The root cap is the structure that detects the pull of gravity and thus controls the downward growth of roots (Petricka et al., 2012). Statocytes are specialized root-cap cells that contain amyloplasts, which will precipitate if the root is reoriented (Kadereit et al., 2014). Cells in the elongation zone elongate and allow root growth (Crang et al., 2018). Root growth is regulated and fine-tuned by several phytohormones. The first phytohormone to be discovered was auxin, which is crucial for cell elongation and lateral root growth (Petricka et al., 2012).

Light is one of the most important environmental factors for plant development. Light cues of varied intensity and quality cause plants to change their morphological traits (Yadav et al., 2020). Besides that, light and temperature also modulate phytochrome growth via phytochrome (Ibrahim and František, 2022). Light perceived by photosensory systems in above-ground tissues can affect the roots via long-distance signal transduction pathways (Qu et al., 2017). Sunlight, on the other hand, can reach root tissues that are several centimeters underground (Qu et al., 2017). Plants use dedicated photoreceptors to receive light signals of various wavelengths. Activated photoreceptors trigger a signal transduction cascade, which results in a wide range of gene expression modifications that affect physiological and developmental responses (Su et al., 2017). Most known plant photoreceptors, including phytochromes, cryptochromes, phototropins, and ultraviolet receptors (UVR), are expressed in the root tissues (Qu et al., 2017). Phytochromes are a class of red (R)/far-red (FR) light photoreceptors in plants that mediate the expression of various genes and are involved in root development and structure (Briggs et al., 2001).

When seedlings receive light, the elongation of the hypocotyls is carefully regulated to match the intensity and quality of light around them, and the phenomenon of de-etiolation occur, in which the development of leaves and chloroplasts inhibits stem elongation and promotes root growth and lateral root development, a process known as photomorphogenesis. The initial response of plants to light is photomorphogenesis, in which the shoot and root meristems are activated, and a series of changes, such as cell division and expansion, lead to changes in the differentiation structure and function of plant cells, and eventually the formation of tissues and organs (McNellis and Deng, 1995).

Light, as we have seen, has a rapid and dramatic impact on root development and physiology. Light is shown to have a great impact on adventitious roots and hypocotyles (Zeng et al., 2022). That aspect should be taken into account while doing experiments with plants, particularly those focusing on roots. Seeds are usually planted in transparent agar medium in hyaline Petri dish plates in laboratory settings, exposing roots and shoots to light in a similar way. Sucrose is also added to the growth medium of the classic agar plate culture technique (TPG, traditional plant-growing). However, because this is not a natural environment for roots, certain artifacts may occur (Xu et al., 2013). Improved approaches are available to make root experiments more efficient. An improved agar-plate method (IPG, improved plant-growing) is one example, in which shoots are lighted while roots are grown in a media without sucrose under dark circumstances. When comparing IPG to TPG, the root and lateral root lengths are both shorter, and the root hair density is lower. The primary root, on the other hand, was much longer. As a result, IPG provides a better and more natural environment for investigating *A. thaliana* root development and responses (Xu et al., 2013).

The target of rapamycin (TOR) is a large and highly conserved protein belonging to the family of phosphatidylinositol 3-kinase-related kinases (PIKKs). In response to environmental changes such as nutrients, energy status, and growth factors, TOR serves as a key sensor of cell growth and metabolism. Recent research has discovered that the conserved TOR pathway is vital in coordinating plant development at the whole plant level (Barrada et al., 2015). Furthermore, the Arabidopsis genome seems to have a single critical TOR gene, which down-regulation results in reduced plant growth, stress resistance (Menand et al., 2002), and increased life span (Ren et al., 2013). Moreover, *Arabidopsis* plants silenced for TOR expression display significantly reduced polysome abundance (Deprost et al., 2007), indicating that TOR plays a function in plant translational regulation. TOR inhibitors restrict the meristematic cell proliferation capability by reducing the number of cells in the MZ, mostly via encouraging differentiation (Montané and Menand, 2013). One of the most effective TOR inhibitors is AZD. As a second-generation mTOR inhibitor (known as ATP-competitive mTOR kinase inhibitor), it is developed not only to suppress mammalian TOR for cancer therapy but also to inhibit TOR in plants. AZD can bind to the TOR kinase domain within the ATP-binding pocket and inactivates the TOR complex (Montané and Menand, 2013). The aim of this study was to show the effect of AZD on Arabidopsis seedlings grown for 96 h under different light conditions. We could show that when Arabidopsis is treated with AZD and grown for 96 h under different light conditions, the root and hypocotyl are significantly modulated.

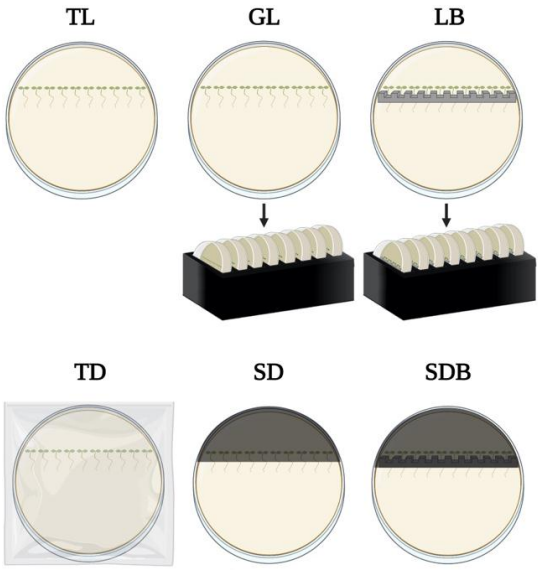

Plate 1. Experimental setup performed in this study: Different light conditions for *A. thaliana* seedlings growth. First line from left to right: total light (TL), gradient light (GL), light blocker (LB). Second line from left to right: total dark (TD), shoot dark (SD), shoot dark with blocker (SDB).
Source: Authors

MATERIALS AND METHODS

Arabidopsis thaliana seedlings grown under different light conditions

Growth media preparation

The growth medium was prepared by mixing the MS medium salt (with vitamins), saccharose and dH_2O. After adding each to a 1 L container, the pH was adjusted to 5.8 using KOH or HCl. After that, 4 g of phytagel was added to 1 L. The medium was mixed and autoclaved at 120°C. The medium was placed in Petri dishes of different sizes and prepared under a sterile bench, for further usage. For the stupor experiment with *A. thaliana* seedlings, medium was added on round Petri dishes with AZD at 5 µM concentration.

Seeds preparation

A. thaliana seeds were sterilized in a plastic tube for 3 min with 1 mL of 70% ethanol. This was followed by a 5 min treatment with 1 mL sodium hypochlorite solution. The plastic tube was inverted many times in each phase. The seeds were washed five times in distilled water. Sterilized seeds were sown on square Petri dishes with ½ MS medium under the sterile bench. The square Petri dishes with sterilized seeds were stored in the fridge for stratification for 48 h at 4°C and transferred to the growth chamber for 96 h for seed germination.

Experimental preparation with AZD

To investigate the influence of AZD on *A. thaliana* root and hypocotyl growth, *A. thaliana* seedlings were transferred to round Petri dishes with phyto agar and AZD (5 µM). The 48 h stratified seedlings were placed side by side with straightened roots in a horizontal position. Control plates were treated in the same way but, only containing phyto agar. After placing the seedlings, all dishes were sealed with parafilm and then transferred to different light conditions (Plate 1). Each treatment was repeated in triplicate. The six light conditions used are as follows: (1) Total light (TL): Round Petri dishes with *A. thaliana* seedlings were placed under the light of the growth chamber with the intensity of 100 µmol s^{-1} m^{-2}. (2) Total dark (TD): Plants were kept in total darkness (covered with aluminum foil) for 96 h. Moreover, shaded seedling roots create two forms of light; gradient light and light blocker. Shoot dark and shoot dark with a light blocker were two types of light conditions created by shading seedling shoots. (3) Gradient light (GL): Plants in the Petri dish were introduced in a black box, where the roots were inside the box and the hypocotyl outside, resulting in a slight gradient with a value of 39.74 µmol s^{-1} m^{-2}. (4) Light blocker (LB): A light blocker strip was placed inside the medium, perpendicular to the Petri dish, preventing light from reaching below the blocker. Subsequently, they were introduced into a black box, resulting in light intensity of 7.27 µmol s^{-1} m^{-2}. (5) Shoot dark (SD): The hypocotyls of *A. thaliana* were covered resulting in light intensity of 7.91 µmol s^{-1} m^{-2}. (6) Shoot dark with light blocker (SDB): The light blocker strip (same as LB) was placed on medium in a round Petri dish and then the hypocotyls of the seedlings were covered, resulting in light intensity of 2.03 µmol s^{-1} m^{-2}.

Root and hypocotyl lengths measurements

After 24, 48, 72 and 96 h the round Petri dishes were scanned. Based on the digital images, the root length and hypocotyl length were measured via Fiji software.

Skototropism experimental preparation

To investigate the influence of distance to darkness on *A. thaliana* roots for the skototropism experiment, *A. thaliana* seedlings were transferred to round Petri dishes with phyto agar. The seedlings were placed in a vertical position, one below the other with straightened roots. After placing the seedlings, all dishes were sealed with parafilm and then placed in construction that held one-half of the Petri dish in darkness. Dishes were aligned in the construction and set with different distance patterns (0, 10 and 20 mm) from the *A. thaliana* seedlings to the darkness and then placed under artificial light (100 µmol s^{-1} m^{-2}) for 96 h in the growth chamber.

Measurements and evaluation

After 96 h, the round Petri dishes were scanned. Based on the digital images, the root bending angle was measured. Values for root bending were sorted into 3 groups: (1) Positive values, showing a bending towards darkness; (2) Negative values, indicating a bending away from darkness; (3) A group zero, exhibiting no visible behavior towards or away from light. Collected data for the experiment were evaluated with Fiji ImageJ software. The length standard for these measurements was set with the help of a ruler which was calibrated with the respective samples. Statistical analysis was performed using Graphpad Prism (version 9.1.1)

RESULTS

Treatment with AZD (5 µM) under shaded light conditions

We found that the growth of the AZD treatment groups

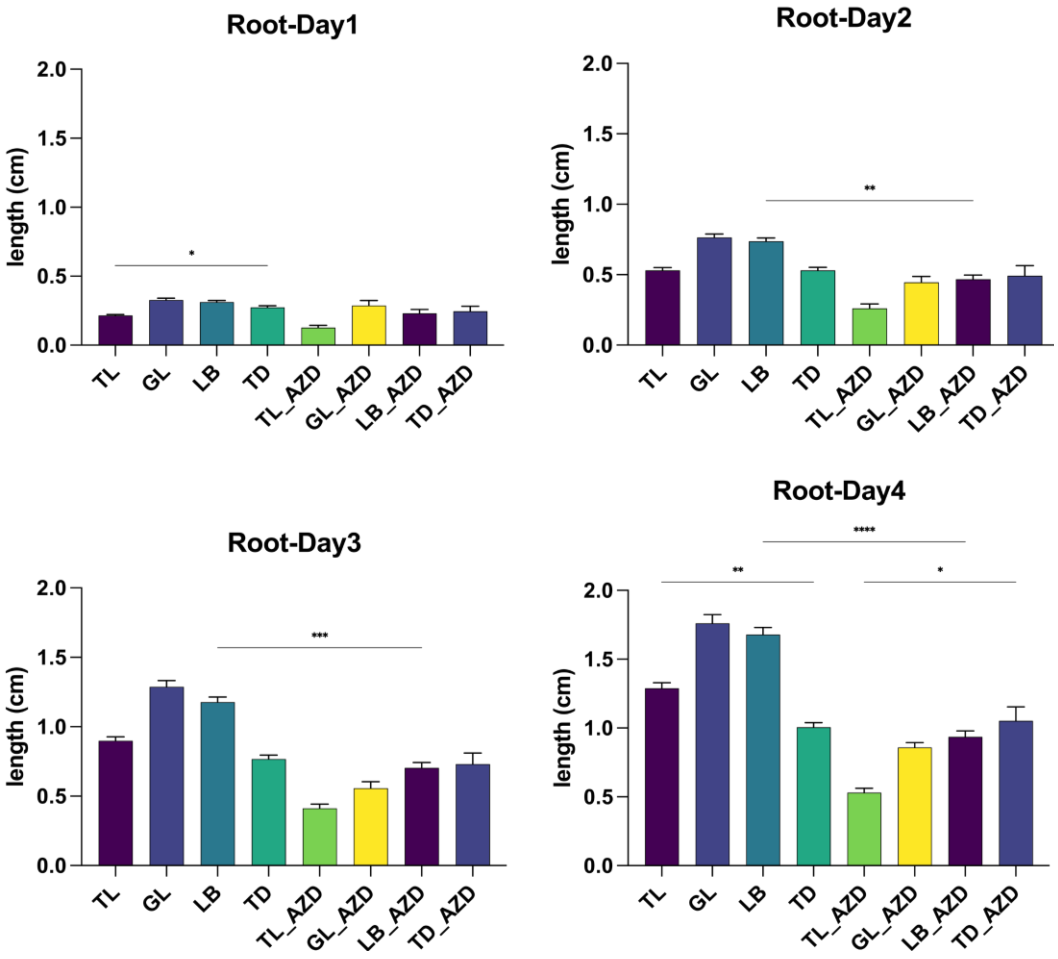

Figure 1. The root length of *A. thaliana* seedlings was measured for 24, 48, 72 and 96 h. The x-axis shows the seedlings were grown for Control as well as AZD [5μM] treatments under different light conditions. The y-axis represents the average root length in cm. Bars in different colors represent different light conditions.
Source: Authors

was substantially slower than the control groups, but no significant difference was seen in the total dark condition (TD). For control groups, the root length in the total dark condition was always the shortest compared with that in other lighting conditions, and in the gradient light (GL) and light blocker (LB) settings. Importantly, root lengths were longer in the gradient light (GL) and light blocker (LB) conditions than in the total light condition (TL). This shows that root growth speeds up if it grows within light-dark gradients and also there is a clear inhibitory role of AZD in root growth. Figure 1 shows a clear difference after four days of growth.

Root growth under different light conditions

When comparing the hypocotyl length in different illumination conditions under the same treatment, it was noted that the length of hypocotyls under total dark conditions (TD) was much larger than that under other illumination conditions and that the length of hypocotyls under complete illumination was always the shortest. Furthermore, there was no significant difference in hypocotyl development between the control and AZD treatment groups (Figure 2). This result shows that AZD has no significant influence on hypocotyl growth under our studied condition.

Hypocotyl growth under different light conditions

Shoot-shaded light conditions

Seedling root and hypocotyl growth of the control group and AZD treatment group was compared under shoot-shaded light conditions (Figures 3 and 4). The root growth of the AZD treatment group was significantly slower than that of the control group. Moreover, root

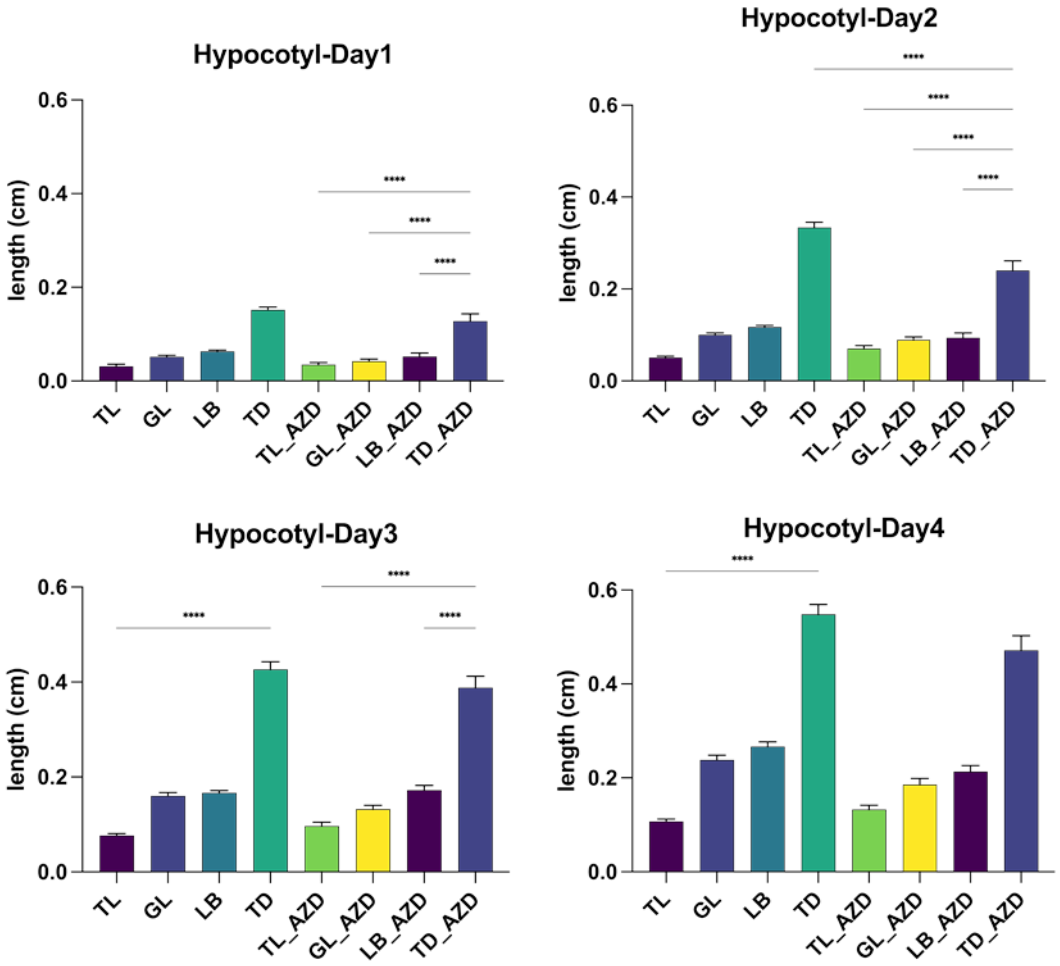

Figure 2. Hypocotyl length of *A. thaliana* seedlings was measured for 24, 48, 72 and 96 h. The x-axis shows the seedlings were grown for Control as well as AZD (5 μM) treatments under different light conditions. The y-axis represents the average root length in cm. Bars in different colors represent different light conditions.
Source: Authors

development of shoot dark (SD) condition was faster than shoot dark with light blocker (SDB) condition. Importantly, after 96 h of development, the root growth length in the AZD treatment group was less than 0.2 cm under different light conditions, far less than the control group (Figure 3).

Root growth under different light conditions

In total light conditions (TL), hypocotyl development was slower than in the other two light conditions (SD, SDB). For the control treatment, the hypocotyl length increased more as the hypocotyl light intensity declined, as determined by comparing hypocotyl development under shoot dark (SD) and shoot dark with light blocker (SDB) conditions. For AZD treatments, it is worth mentioning that hypocotyl growth in the SD condition is faster than that in the SDB condition (Figure 4).

DISCUSSION

Arabidopsis was selected as a model plant about decades ago because of the unique traits that made it ideal for laboratory research. *Arabidopsis* has been cultivated on Petri dishes since then, and the vast majority of root biology research has been done with the root system exposed to light. Light appears to have a direct influence on root development and responses, according to recent research (Yokawa et al., 2014; Meng, 2015). Our results have revealed a role for light in both root growth and hypocotyl growth. Six different light conditions (total light, gradient light, light blocker, total dark, shoot dark, shoot dark with blocker) were set up since the influence of light on seedling growth and differentiation can be divided into direct and indirect aspects. The light conditions (shoot dark and shoot dark with blocker) are the indirect ways to explore the influence of light on root growth via changing the light

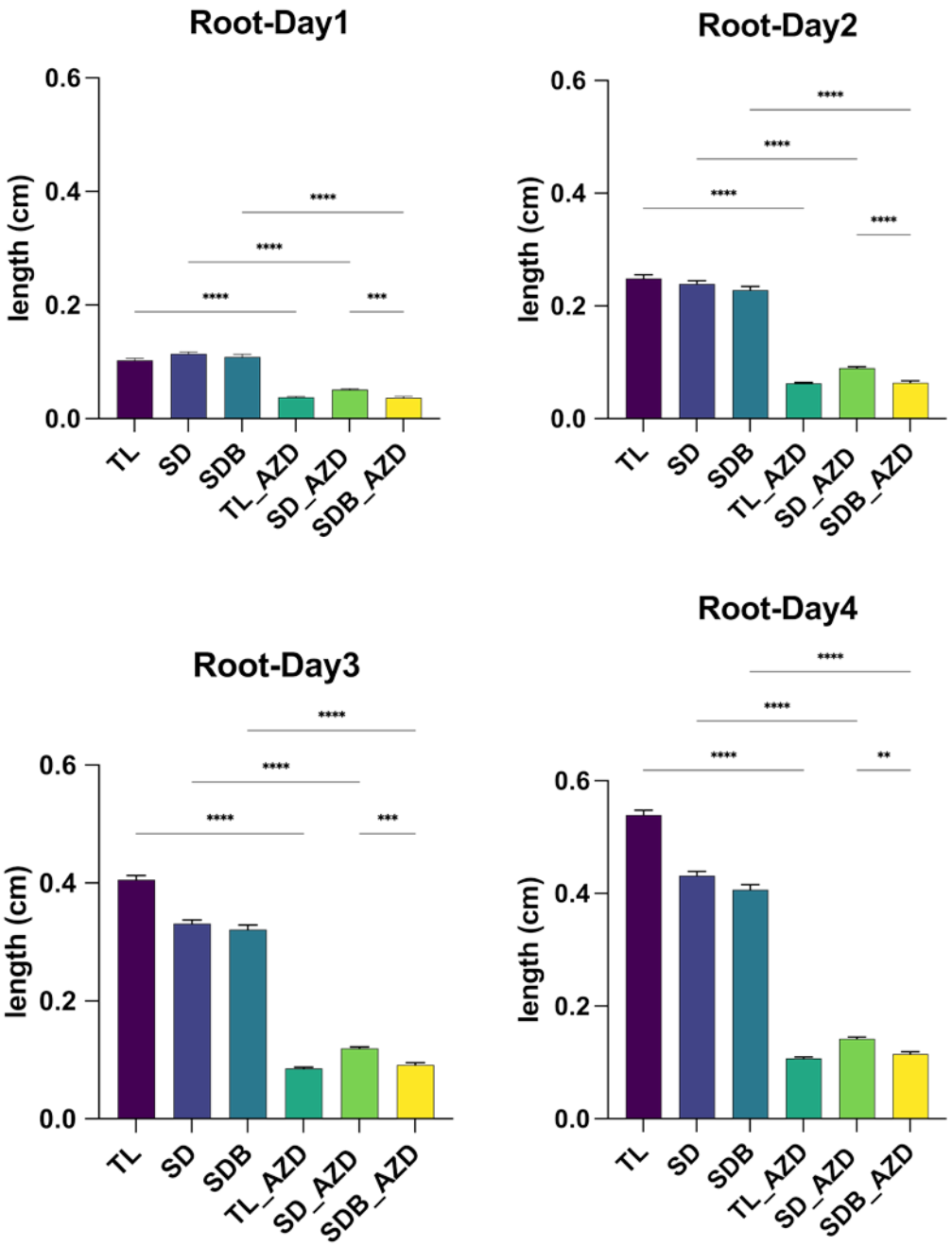

Figure 3. The root length of *A. thaliana* seedlings was measured for 24, 48, 72 and 96 h. The x-axis shows the seedlings were grown for Control as well as AZD (5 μM) treatments under different light conditions. The y-axis represents the average root length in cm. Bars in different colors represent different light conditions.
Source: Authors

intensity on the shoot. The investigations have found that the total root length under shoot dark (light intensity 7.91 μmol s^{-1} m^{-2}) and shoot dark with blocker (light intensity 2.03 μmol s^{-1} m^{-2}) circumstances was substantially less than under total light conditions. Within 24 and 48 h, there was no significant difference in root length across the three lighting conditions (SD, SDB and TL), but from 72 to 96 h, the total light condition had a considerably longer root length than the other two illumination conditions. This situation can be explained by the fact that photosynthesis mainly occurs in plant shoots, and plants are unable to produce enough organic matter (sucrose) to fulfill their growth requirements after a period of limited light. Yokawa et al. (2011) reported on the root-

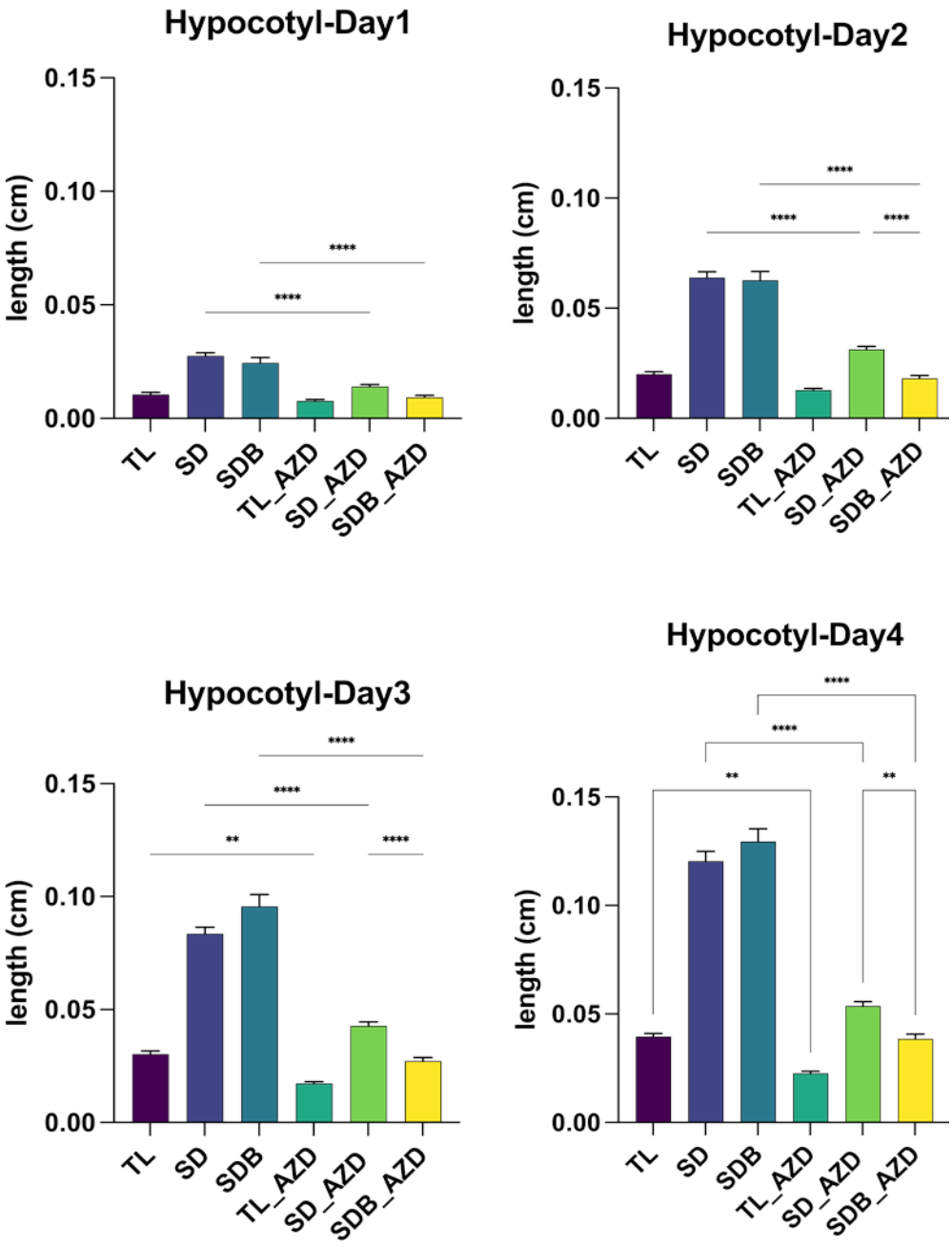

Figure 4. Hypocotyl length of *A. thaliana* seedlings was measured for 24, 48, 72 and 96 h. The x-axis shows the seedlings were grown for Control as well as AZD (5 µM) treatments under different light conditions. The y-axis represents the average hypocotyl length in cm. Bars in different colors represent different light conditions.
Source: Authors

shoot ratio of *Arabidopsis* seedlings growing in the soil (whose roots are almost completely dark) is 1:1. The exposure of roots to light causes stress in the entire plant, and roots normally respond by increasing their growth. This indicates that illumination of the roots disturbs the balance of the root-shoot ratio, which is approximately 1:1 in a normal physiological situation. The analysis of our experimental data also supported this conclusion. The gradient light condition had a higher light intensity than the simulated natural condition (light blocker), and the gradient light condition had a longer root length than the light blocker condition. Meanwhile, in the gradient light condition, the hypocotyl length was less than in the light blocker condition. Most *Arabidopsis*

studies are conducted out in transparent Petri dishes, ignoring the extra effects that the additional light may have on the roots. Results reported the root length under total light conditions was significantly shorter than that under gradient light and simulated natural conditions (light blocker), confirming the shortcomings of the traditional plant-growing (TPG) technique. Silva-Navas et al. (2015) demonstrated root illumination shortens root length and increases the early development of lateral roots, promoting root system expansion. Hypocotyl is a highly plastic organ whose length is controlled by a network of interacting elements including light and plant hormones (Vandenbussche et al., 2005). In continuous darkness, the process of hypocotyl elongation differs significantly from that in uniform light. TOR is critical for plant translational control (Méndez-Gómez et al., 2022). Translation re-initiation at upstream ORFs (uORFs) in genes that play crucial roles in stem cell control and organogenesis in plants is significantly reliant on TOR (Schepetilnikov et al., 2017). Many important proteins are encoded by uORF-mRNAs, including transcription factors, protein kinases, cytokines, and growth factors. The results from the study indicated that seedlings of *A. thaliana* treated with AZD (an ATP-competitive inhibitor of TOR) efficiently inhibited root and hypocotyl growth when compared to plants grown under control conditions. Our findings are consistent with previous research, which indicated that at the whole plant level, AZD treatment of *A. thaliana* delayed cotyledon and leaf development while also shortening root length (Montané and Menand, 2013). The situation is assumed to occur because AZD limits meristem activity in plants and may diminish the size of differentiated cells. Meanwhile, AZD may induce AtTOR haplo-insufficiency which results in reduced plant growth and stress resistance (Montané and Menand, 2013).

The control of root-to-shoot is a complex physiological process in plant. ROS-regulating factor was shown to play a key role in Arabidopsis (Jin et al., 2022). TOR signaling activity, which promotes growth and cell division, may be suppressed in QC. The presence of TOR in both the apical and basal meristems of the root shows that TOR is involved in both root proliferation and cell expansion (Montané and Menand, 2013). Furthermore, Barrada et al. (2015) stated that the TOR kinase is emerging as a key regulator of plant environmental and hormonal responses. TOR increases BR signaling, most likely via a signaling relay mediated by BIN2 substrates (Wu et al., 2019). Interestingly, by comparing the experimental data, it was discovered that hypocotyl length in the control group under shoot dark with blocker condition was larger than that under shoot dark condition; however, it was the opposite after AZD therapy. The outcome can be explained by the following reason: The use of AZD suppresses the activity of TOR, which indirectly affects the BR signaling, leading to a significant influence on the hypocotyl being almost completely dark condition (shoot dark with blocker condition).

Conclusions

A number of conclusions were drawn from this study: (1) That root growth speeds up if it grows within light-dark gradients and AZD shows a clear inhibitory role in root growth. (2) The length of hypocotyls under total dark conditions was much larger than that under other illumination conditions and that the length of hypocotyls under complete illumination was always the shortest. AZD has no significant influence on hypocotyl growth under the studied condition. (3) Root development of shoot dark (SD) condition was faster than shoot dark with light blocker (SDB) condition. Also, after 96 h of development, the root growth length in the AZD treatment group was less than 0.2 cm under different light conditions, far less than the control group (4). For AZD treatments, the hypocotyl growth in the SD condition is faster than that in the SDB condition. This study shows that AZD, a TOR inhibitor, drastically reduced root and hypocotyl length. The findings are consistent with previous research, which indicated that at the whole plant level, AZD treatments of *A. thaliana* delayed cotyledon and leaf development while also shortening root length (Montané and Menand, 2013).

CONFLICT OF INTERESTS

The authors have not declared any conflict of interest.

RECOMMENDATION

Further experiments are needed to pool-down other kinases that may be involved in this pathway.

ACKNOWLEDGMENTS

The authors Xingyu Yan and Felipe Yamashita acknowledge scholarships from Stiftung Zukunft (Germany).

REFERENCES

Baluška F, Mancuso S (2013). Root apex transition zone as oscillatory zone. Frontiers in Plant Science 4:354.

Baluška F, Mancuso S, Volkmann D, Barlow PW (2010). Root apex transition zone: A signalling-response nexus in the root. Trends in Plant Science 15(7):402-408.

Brand U, Hobe M, Simon R (2001). Functional domains in plant shoot meristems. BioEssays 23(2):134-141.

Briggs WR, Olney MA (2001). Photoreceptors in plant photomorphogenesis to date. Five phytochromes, two cryptochromes, one phototropin, and one superchrome". Plant Physiology 125:85-88.

Crang R, Lyons-Sobaski S, Wise R (2018). A concept-based approach to the structure of seed plants. Plant Anatomy. doi: 10.1007/978-3-319-77315-5.

Deprost D, Yao L, Sormani R, Moreau M, Leterreux G, Nicolaï M, Bedu M, Robaglia C, Meyer C (2007). The *Arabidopsis* TOR kinase links plant growth, yield, stress resistance and mRNA translation. EMBO

Reports 8(9):864-870.
Ibrahim N, František B (2022). The role of N-terminal module of PhyB in modulating root and hypocotyl growth length in Arabidopsis. African Journal of Biotechnology 21(6):287-291.
Jin T, Wu H, Deng Z, Cai T, Li J, Liu Z, Waterhouse PM, White RG, Liang D (2022). Control of root-to-shoot long-distance flow by a key ROS-regulating factor in *Arabidopsis*. Plant, Cell and Environment 45(8):2476-2491.
Jürgens G, Mayer U, Ramon A TR, Berleth T, Miséra S (1991). Genetic analysis of pattern formation in the Arabidopsis embryo. Development 113 :27-38
Kadereit J.W, Körner C, Kost B, Sonnewald U (2014). *Strasburger - Lehrbuch Der Pflanzenwissenschaften*. Berlin, Heidelberg: Springer Berlin Heidelberg.doi: 10.1007/978-3-642-54435-4.
McNellis TW, Deng XW (1995). Light control of seedling morphogenetic pattern". Plant Cell 7(11):1749-1761.
Menand B, Desnos T, Nussaume L, Berger F, Bouchez D, Meyer C, Robaglia C (2002). Expression and disruption of the *Arabidopsis* TOR (target of rapamycin) gene. Proceedings of the National Academy of Sciences of the United States of America 99(9):6422-6427.
Méndez-Gómez M, Castro-Mercado E, Peña-Uribe CA, Reyes-de la Cruz H, López-Bucio J, García-Pineda E (2020). Target of rapamycin signaling plays a role in Arabidopsis growth promotion by Azospirillum brasilense Sp245. Plant Science 293:110416.
Meng LS (2015). Transcription coactivator *Arabidopsis* ANGUSTIFOLIA3 modulates anthocyanin accumulation and light-induced root elongation through transrepression of Constitutive Photomorphogenic1. Plant Cell and Environment 38(4):838-851.
Montané MH, Menand B (2013). ATP-competitive mTOR kinase inhibitors delay plant growth by triggering early differentiation of meristematic cells but no developmental patterning change. Journal of Experimental Botany 64(14):4361-4374.
Petricka JJ, Winter CM, Benfey PN (2012). Control of *Arabidopsis* root development". Annual Review of Plant Biology 63:563-590.
Qu Y, Liu S, Bao W, Xue X, Ma Z, Yokawa K, Baluška F, Wan Y (2017). Expression of root genes in *Arabidopsis* seedlings grown by standard and improved growing methods. International Journal of Molecular Sciences 18:951.
Ren M, Venglat P, Qiu S, Feng L, Cao Y, Wang E, Xiang D, Wang J, Alexander D, Chalivendra S, Logan D (2013). Target of rapamycin signaling regulates metabolism, growth, and life Span in *Arabidopsis*. Plant Cell 24(12):4850-4874.
Schepetilnikov M, Makarian J, Srour O, Geldreich A, Yang Z, Chicher J, Hammann P, Ryabova LA (2017). GTPase ROP2 binds and promotes activation of target of rapamycin, TOR, in response to auxin. The EMBO Journal 36(7):886-903.
Silva-Navas J, Moreno-Risueno MA, Manzano C, Pallero-Baena M, Navarro-Neila S, Téllez-Robledo B, Garcia-Mina JM, Baigorri R, Gallego FJ, del Pozo JC (2015). D-Root: a system for cultivating plants with the roots in darkness or under different light conditions. Plant Journal 84(1): 244-255.
Su J, Liu B, Liao J, Yang Z, Lin C, Oka Y (2017). Coordination of cryptochrome and phytochrome signals in the regulation of plant light responses. Agronomy 7(1):25.
Vandenbussche F, Pierik R, Millenaar FF, Voesenek LA, Van Der Straeten D (2005) Reaching out of the Shade. Current Opinion in Plant Biology 8(5):462-468.
Verbelen JP, Cnodder TD, Le J, Vissenberg K, Baluška F (2006). The root apex of *Arabidopsis thaliana* consists of four distinct zones of cellular activities: meristematic zone, transition zone, fast elongation zone, and growth terminating zone. Plant Signaling and Behavior 1(6):296-304.
Wu Y, Shi L, Li L, Fu L, Liu Y, Xiong Y, Sheen J (2019). "Integration of nutrient, energy, light, and hormone signalling via TOR in plants. Journal of Experimental Botany 70(8):2227-2238.
Xu W, Ding G, Yokawa K, Baluška F, Li QF, Liu Y, Shi W, Liang J, Zhang J (2013). An improved agar-plate method for studying root growth and response of *Arabidopsis thaliana*. Scientific Reports 3:1273.
Xu W, Ding G, Yokawa K, Baluška F, Li QF, Liu Y, Shi W, Liang J, Zhang J (2020). Light signaling and UV-B-mediated plant growth regulation. Journal of Integrative Plant Biology 62(9):1270-1292.
Yokawa K, Fasano R, Kagenishi T, Baluška F (2014). Light as stress factor to plant roots-case of root halotropism. Frontiers in Plant Science 5:718.
Yokawa K, Kagenishi T, Kawano T, Mancuso S, Baluška F (2011). Illumination of *Arabidopsis* roots induces immediate burst of ROS production". Plant Signaling and Behavior 6(10):1460-1464.
Zeng Y, Schotte S, Trinh HK, Verstraeten I, Li J, Van de Velde E, Vanneste S, Geelen D (2022). Genetic Dissection of Light-Regulated Adventitious Root Induction in *Arabidopsis thaliana* Hypocotyls. International Journal of Molecular Sciences 23(10):5301.

Vol. 12(2) pp. 31-40, July-December 2022
DOI: 10.5897/IJBMBR2022.0328
Article Number:9C6335070062
ISSN 2141-2154
Copyright © 2022
Author(s) retain the copyright of this article
http://www.academicjournals.org/IJBMBR

ACADEMIC JOURNALS

International Journal of Biotechnology and Molecular Biology

Full Length Research Paper

Gene regulating effects of *Cymbopogon citratus* on glucose metabolism of normal albino rats

Adegbegi Ademuyiwa Joshua[1]*, Onoagbe Iyere Osalase[1] and Omonkhua Akhere Akuekegbe[2]

[1]Department of Biochemistry, Faculty of Life Sciences, University of Benin, Benin City, Edo State, Nigeria.
[2]Department of Medical Biochemistry, School of Basic Medical Sciences, University of Benin, Benin City, Edo State, Nigeria.

Received 7 March, 2022; Accepted 14 September, 2022

Cymbopogon citratus **has been reported to have hypoglycaemic and antidiabetic activities. This study evaluates the insulinotropic properties of *C. citratus* via gene expression. *C. citratus* was administered to normal rats as pulverized leaves (2, 10 and 30%) mixed with animal feed for one week; as aqueous and ethanol extracts at a dosage of 30 and 100 mg/kg body weight for 30 days; and as isolated saponins, flavonoids and tannins at 30 µg/kg for 7 days. Animals were sacrificed after the treatment protocol and organs of interest removed for analysis. Gene expression analysis of *C. citratus* was based on polymerase chain reaction (PCR) for glucagon like peptide-1 (GLP-1), insulin, glucose transporter 4 (GLUT4) and potassium ion gated channel (KCNJ5), using isolated mRNA. Results showed that the extracts and phytochemicals fractions (particularly flavonoids) of *C. citratus* increased insulin gene expression, whereas only the whole plant feeding of normal rats increased GLP-1 gene expression in a dose-dependent manner. Administration of plant extracts increased GLUT-4 expression while phytochemical fractions of *C. citratus* did not alter the expression of KCNJ5 gene. It can be concluded that the pharmacology of *C. citratus,* especially the whole plant and the aqueous and ethanol extracts, favours the up-regulation of some insulinotropic genes.**

Key word: Insulinotropic properties, *Cymbopogon citratus*, gene expression, insulin, saponins, flavonoids, tannins.

INTRODUCTION

Insulin dysfunction has been described as one of the major contributors to ill health and premature mortality worldwide (WHO, 2019, 2021). This can lead to aberration in glucose metabolism as a result of insulin secretion and action defects (IDF, 2020). Diabetes mellitus is a globally known chronic disease (Al-Lawati, 2017), that occurs either when the pancreas does not produce enough insulin or when the body cannot effectively use the insulin it produces (WHO, 2020). Studies have shown the existence of a complex interaction between inflammation, endoplasmic reticulum stress, oxidative stress, mitochondrial dysfunction and autophagy dysregulation and diabetes mellitus which play important roles in insulin resistance (Cho et al., 2018).

*Corresponding author. E-mail: muyithegreat@yahoo.com. Tel: +234 8066149905.

Author(s) agree that this article remain permanently open access under the terms of the Creative Commons Attribution License 4.0 International License

Insulin controls both the metabolism of carbohydrates and fats by facilitating the absorption of glucose from the blood to skeletal muscles and fat tissue and by promoting fat storage than its usage (Zheng et al., 2018).

It is well known that insulin resistance plays an important role in the onset of diabetes mellitus and that failure of pancreatic β-cells to produce and release insulin is instrumental to the development of hyperglycaemic condition (Einarson et al., 2018). The major role of islets of Langerhans of the pancreatic β-cells is to secrete insulin to control blood glucose homeostasis. Insulin secretion is subject to control by nutrients and hormonal, neural, and pharmacological factors (Di Meo et al., 2016). The alteration of these factors contributes to the pathogenesis of type 1 and type 2 diabetes (Di Meo et al., 2018).

The major gut insulinotropic hormones or incretins is glucagon-like peptide-1 (GLP-1) (Zhang et al., 2017). GLP-1 is produced mainly by the enteroendocrine L cells of the distal intestine in response to nutrient ingestion (Baggio et al., 2018). The mechanism of action of GLP-1 involves its binding to its receptor, which in turn affects blood glucose levels by stimulating insulin secretion, thus inhibiting glucagon secretion, inhibiting gastric emptying and reducing food intake (Burmeister et al., 2017). Its physiological functions range from hypoglycaemic effect, anti-inflammatory, antioxidative, neurogenerative, as well as vascular protective effects in various cells and tissues including the kidney, lung, heart, hypothalamus, endothelial cells, neurons, astrocytes, microglia, and pancreatic beta cells (Drucker et al., 2017; Hou et al., 2016).

Report by Klip et al. (2019) showed that the level of glucose transporter 4 (GLUT-4) expression determines the maximal effect of insulin on glucose transport. Thus, diabetes leads to suppression at a pre-translational step resulting in a marked decrease in GLUT-4 expression in skeletal muscle and adipose tissue (Lauritano and Ianora, 2016). Potassium Voltage-Gated Channel Subfamily J Member 5 (KCNJ5) is an example of ATP-sensitive K^+ gated channels, which plays an important role in electrogenic events within the cell (Wang et al., 2021). KCNJ5 is sensitive to metabolic changes in the pancreatic β-cell, coupling cellular metabolism to electrical activity and to insulin secretion (Wang et al., 2021). Invariably, when K^+ channels channels are opened, β-cell repolarise and insulin secretion is suppressed, leading to diabetic state, and when it is closed, β-cell depolarise and insulin secretion is activated (Wu et al., 2019).

Cymbopogon citratus is a well-known medicinal herb in tropical and subtropical countries, used as a medicine because of its wide-ranging therapeutic properties (Coelho et al., 2016; Lawal et al., 2017). Studies have shown that *C. citratus* has antibacterial, antifungal, anti-inflammatory, antimalarial, anti-protozoan, and ascaricidal effects (Bello et al., 2019). This medicinal plant has also been reported to have hypocholesterolaemic, hypoglycaemic, hypolipidaemic, anticancer, anti-hypertensive, free radical scavenging and antioxidant properties (Ajayi et al., 2016; Coelho et al., 2016). *C. citratus* have been reported to reduce the fasting and postprandial blood sugar levels, bringing them towards normal and healthy state (Ajayi et al., 2016). The plant have been said to have hypoglycaemic property via insulin synthesis and secretion or increased peripheral glucose utilization (Lawal et al., 2017).

Certain plants phytochemicals such as saponins, tannins, flavonoids, and others, have been shown to possess medicinal properties for instance, certain bioactive compounds of *C. citratus* displayed over 60% inhibition of reactive oxidative species (ROS) generation with increased glucose metabolism and utilization (Ajayi et al., 2016; Coelho et al., 2016). To better understand the effect of *C. citratus* on glucose metabolism, especially in relation to stimulation of insulin production, this study assessed its effect on some genes with insulinotropic effects.

MATERIALS AND METHODS

Plant collection and preparation

C. citratus was harvested from a farm in Akure and authenticated in the Department of Plant Science and Biotechnology, University of Benin. A herbarium specimen with voucher number UBH-C451, was deposited in the University of Benin herbarium. *C. citratus* leaves were washed in clean water three times, sliced and spread on a clean surface at room temperature for two weeks. The dried leaves were milled and sieved into a powdered sample.

Extraction of *C. citratus*

A slight modification of Onoagbe and Esekheigbe (1999) method was used to prepare the extract. The powdered leaves of the plant were used. Two different weights of 1 kg each were soaked in distilled water (aqueous extract) and absolute ethanol (ethanol extract) with continuous stirring for 72 h in a glass container and covered with cheesecloth. At the end of the third day, they were filtered through two layers of cheesecloth and later with a filter paper to completely remove residues. The filtrate was concentrated by a rotary evaporator, and then evaporated to dryness in a freeze dryer. The dried extract was weighed and stored in an air-tight container and kept in the freezer until use.

Isolation of phytochemicals

Solvent extraction of dried powder (500 g) of *C. citratus* was done each for flavonoids by the method described by Subramanian and Nagarjan (1969); saponins by Woo et al. (1980); and tannins by Wall et al. (1996).

Animal ethical clearance

Treatment of the animals was in accordance with the Principle of Laboratory Animal Care. The Local ethical approval was received

from the Ethics Committee, Faculty of Pharmacy, University of Benin, Benin City, Nigeria, with reference number EC/FC/FP/020/020.

Experimental design

Effect of C. citratus leaves on normal rats

Sixteen Wistar rats in four groups of four rats each were given *C. citratus* leaves mixed with their feed for one week using the experimental design: Normal control received 100% normal rat chow, other groups received 2, 10 and 30% *C. citratus* in rat chows.

Effect of aqueous and ethanol extracts of C. citratus on normal rats

Twenty Wistar rats in five groups of four rats each were given *C. citratus* extracts administered for thirty days using the experimental design: Normal control received 100% normal rat chow, other groups received 30 mg/kg body weight (bw) and 100 mg/kg bw of aqueous extracts of *C. citratus* and 30 and 100 mg/kg bw ethanol extracts of *C. citratus*

Effect of saponins, flavonoids and tannins extracted from C. citratus on normal rats

Sixteen Wistar rats in four groups of four rats each were given *C. citratus* isolated photochemical for one week using the experimental design: Normal control received 100% normal rat chow, 30 µg/kg bw saponins, 30 µg/kg bw flavonoids, and 30 µg/kg bw tannins isolated from *C. citratus*

Gene expression

After the final treatment, the animals were sacrificed and mRNA was isolated from the rat liver, ileum, kidney and pancreas, with TRIzol Reagent (Thermo Fisher Scientific) converted to cDNA using Proto Script First Strand cDNA Synthesis Kit (NEB). PCR amplification was done using OneTaq® 2X Master Mix (NEB) using the following primer set: GLP-1 (Forward 5'-3'-ACCGTTTACATCGTGGCTGG; Reverse 5'-3'-CCCTGTGAATGGCGTTTGTC); Insulin (Forward 5'-3'-GAGGCTCTGTACCTGGTGTG; Reverse 5'-3'-ACCTCCAGTGCCAAGGTTT); GLUT4 (Forward 5'-3'-TCTCCGGTTCCTTGGGTTGT; Reverse 5'-3'-TTCCCCATCTTCAGAGCCGAT); β-actin (Forward 5'-3'-ACACTTTCTACAATGAGCTGCG; Reverse 5'-3'-CCAGAGGCATACAGGACAAC); KCNJ5 (Forward 5'-3'-CGACCAAGAGTGGATTCCTT; Reverse 5'-3'-AGGGTCTCCGCTCTCTTCTT).

Gene expression study data analysis

The intensities of the bands from agarose gel electrophoresis were quantified densitometrically using ImageJ software. Pymol was used to visualize the mRNA.

RESULTS

The inclusion of *C. citratus* powder in rat's diet, administration of its aqueous and ethanol extracts as well as saponins, flavonoids and tannins fractions caused significant alteration in insulinotropic gene expression of normal rats. Thus, the potential of *C. citratus* to activate the release of GLP-1 and other target genes to enhance insulin release as observed in this study implies the ability of this plant to produce insulinotropic effects. The release of insulin from the pancreatic ß cells through GLP-1 gene modulation by *C. citratus* powder was seen to be dose dependent (Figure 1). Most of the extracts administered did not alter the GLP-1 gene expression (with the exception of aqueous extract at 100 mg/kg body weight) (Figure 2), whereas saponins, flavonoids, and tannins fractions administration caused repression of GLP-1 gene expression in rat ileum (Figure 3). This report is complemented by the activation of insulin gene expression by the aqueous and ethanol extracts (Figures 4 and 5) as well as the flavonoids of *C. citratus*.

From this study, ethanol extract of *C. citratus* caused up-regulation in GLUT-4 expression in the liver cells after 4 weeks of administration (Figure 6). From this present study, administration of saponins, flavonoids, and tannins fractions from *C. citratus* did not alter the expression of KCNJ5 gene (Figure 7) implying that up-regulation of KCNJ5 gene may not be a major pathway for the isolated phytochemicls of *C. citratus* to exert its insulinotropic effect.

Feeding normal rats at different concentrations of *C. citratus* infused feed caused a dose dependent increase in GLP-1 gene expression in the ileum of the rats. The 30% feed formulation caused a nearly three-fold increase (1.2±0.01) compared to control (0.39±0.05).

Aqueous extract at 30 mg/kg bw (0.69±0.02) and ethanol extract at 30 mg/kg bw (0.77±0.03) and 100 mg (0.68±0.02) treated rats showed GLP-1 levels that were mostly comparable with control (0.65±0.05). Meanwhile, aqueous extract at 100 mg/kg bw (0.21±0.01), showed a significant reduction in GLP-1 gene expression in the ileum of rats when compared with control.

Saponins (0.29±0.05), flavonoids (0.43±0.03) and tannins (0.035±0.001) fractions of *C. citratus* at 30 µg/kg bw repressed GLP-1 gene with tannin having most repression and flavonoids the least, when compared with control (0.58 ± 0.04).

All doses of aqueous 30 mg/kg (1.13±0.03) and 100 mg/kg bw (1.14±0.05) and ethanol extracts- 30 mg/kg bw (1.05±0.03) and 100 mg/kg bw (1.18±0.03) of *C. citratus* significantly (p<0.05) increased the expression of the insulin gene in the pancreas of normal rats compared to control (0.68±0.04).

Flavonoids (1.80±0.05) fraction of *C. citratus* at 30 µg/kg caused a significant increase in insulin gene expression when compared with control; meanwhile, saponins (1.21±0.05) and tannins (1.00±0.02) fractions at 30 µg/kg bw showed no significant differences in insulin gene expression when compared with control (1.29±0.03).

The ethanol extract of *C. citratus* at 100 mg/kg bw(0.594±0.08) caused a significant increase in GLUT4

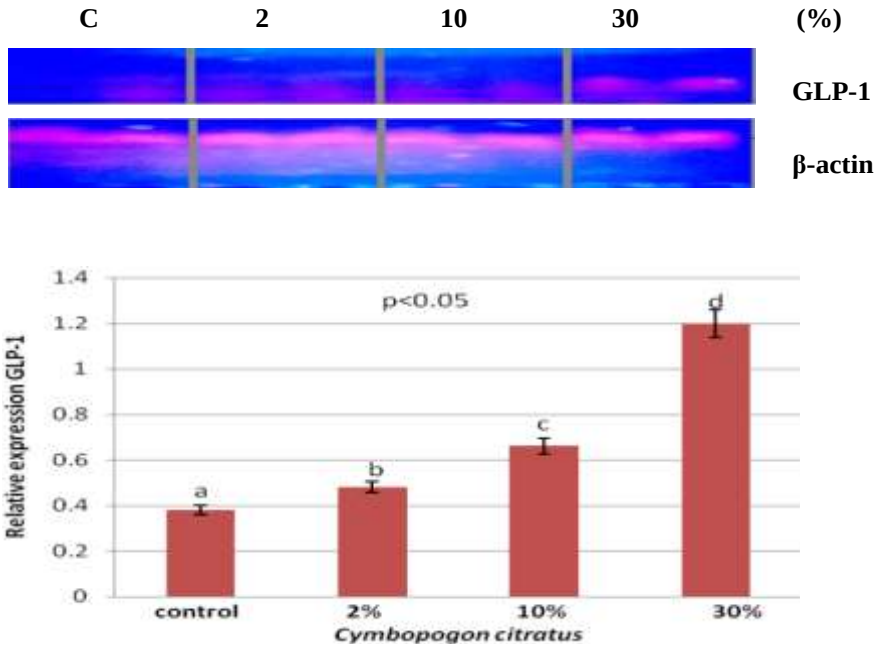

Figure 1. Qualitative-PCR analysis of GLP-1 expression in the ileum of rats fed leaves of *C. citratus* (n= 4) for 7 days at different concentrations. Snapshot representation of RT-PCR and chain reaction-agarose gel electrophoresis was carried on GLP-1 gene followed by densitometric analysis. Values carrying different levels are significantly different at p<0.05.
Source: Kendall and Michael (2010).

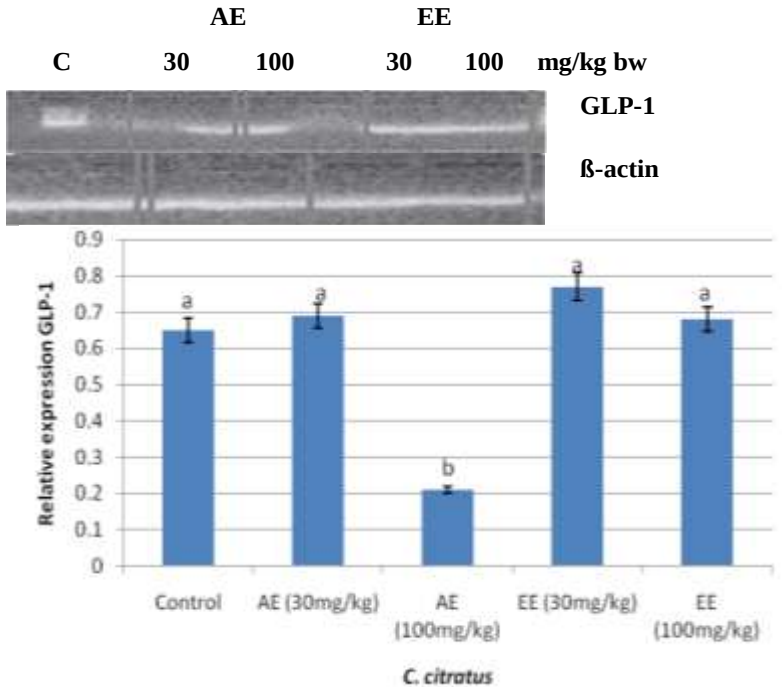

Figure 2. Qualitative-PCR analysis of GLP-1 expression in ileum of rats given aqueous and ethanol extracts of *C. citratus* (n = 4) for 30 days. Snapshot representation of RT-PCR and chain reaction-agarose gel electrophoresis was carried on GLP-1 gene followed by densitometric analysis. Values carrying different levels are significantly different at p<0.05. C= Control; AE= Aqueous extract; EE= Ethanol extract.
Source: Kendall and Michael (2010).

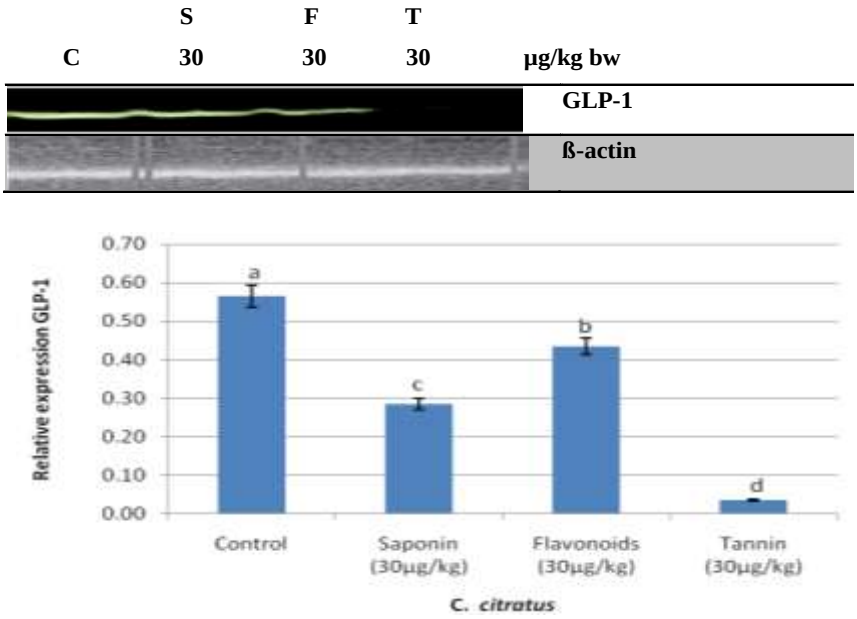

Figure 3. Qualitative-PCR analysis of GLP-1 expression in ileum of rats given saponins, flavonoids and tannins fractions of *C. citratus* (n= 4) for 7 days. Snapshot representation of RT-PCR and chain reaction-agarose gel electrophoresis was carried on GLP-1 gene followed by densitometric analysis. Values carrying different levels are significantly different at $p<0.05$. C= Control; S= Saponins; F= Flavonoids; T = Tannins.
Source: Kendall and Michael (2010).

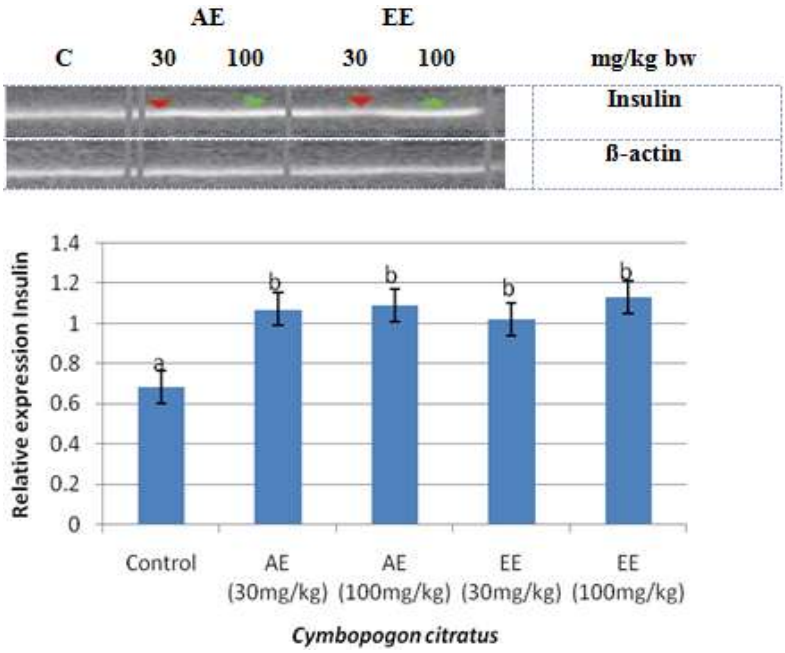

Figure 4. Qualitative-PCR analysis of insulin expression in the pancreas of rats given aqueous and ethanol extracts of *C. citratus* (n= 4) for 30 days. Snapshot representation of RT-PCR and chain reaction-agarose gel electrophoresis was carried on insulin gene followed by densitometric analysis. Values carrying different levels are significantly different at $p<0.05$. C= Control; AE= Aqueous extract; EE= Ethanol extract.
Source: Kendall and Michael (2010).

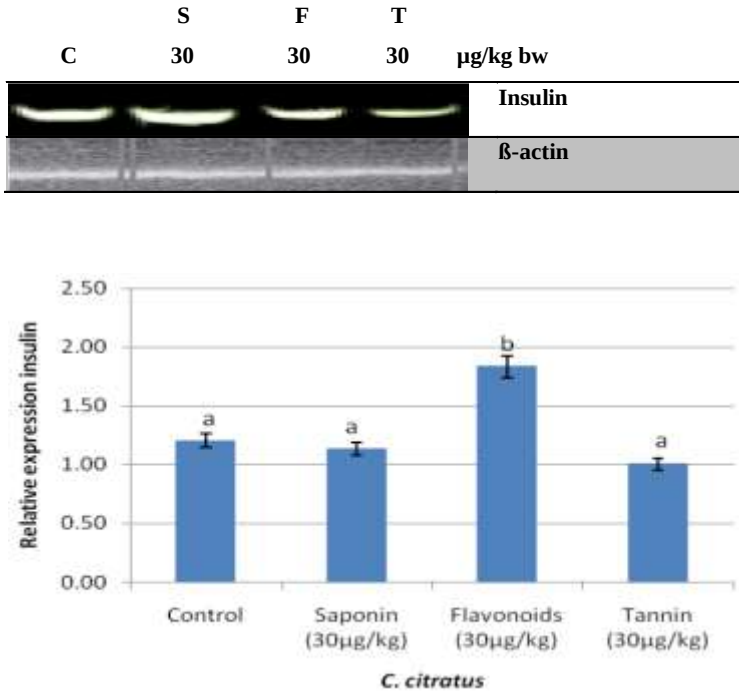

Figure 5. Qualitative-PCR analysis of insulin expression in pancreas of rats given saponins, flavonoids and tannins fractions of *C. citratus* (n= 4) for 7 days. Snapshot representation of RT-PCR and chain reaction-agarose gel electrophoresis was carried on insulin gene followed by densitometric analysis. Values carrying different levels are significantly different at $p<0.05$. C = Control; S = Saponins; F = Flavonoids; T = Tannins.
Source: Kendall and Michael, 2010.

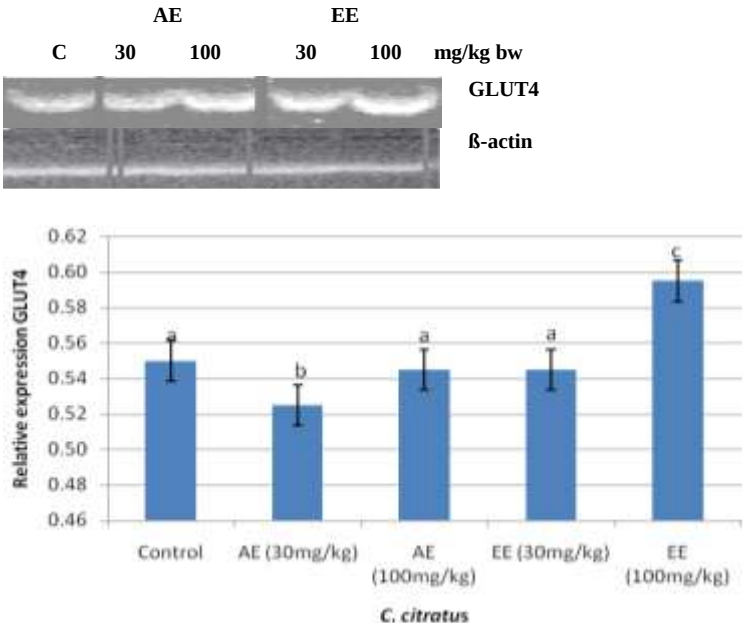

Figure 6. Qualitative-PCR analysis of GLUT4 expression in liver of rats given aqueous and ethanol extracts of *C. citratus* (n= 4) for 30 days. Snapshot representation of RT-PCR and chain reaction-agarose gel electrophoresis was carried on GLUT4 gene followed by densitometric analysis. Values carrying different levels are significantly different at $p<0.05$. C = Control; AE = Aqueous extract; EE= Ethanol extract.
Source: Kendall and Michael (2010).

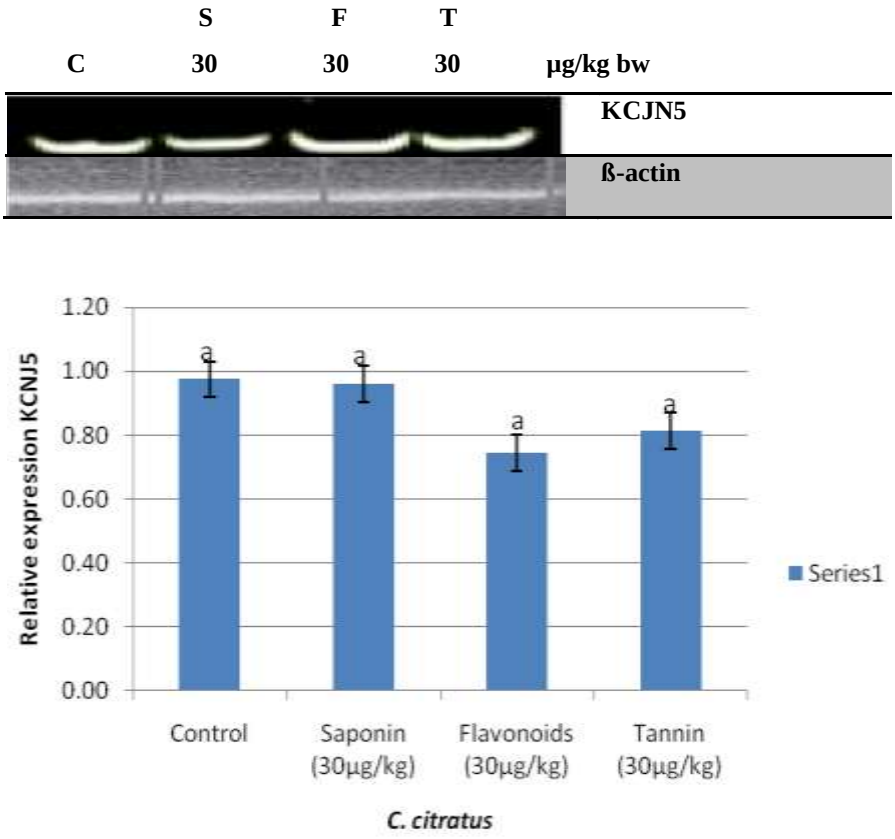

Figure 7. Qualitative-PCR analysis of KCJN5 expression in pancreas of rats given saponins, flavonoids and tannins fractions of *C. citratus* (n= 4) for 7 days. Snapshot representation of RT-PCR and chain reaction-agarose gel electrophoresis was carried on KCJN5 gene followed by densitometric analysis. Values carrying different levels are significantly different at $p<0.05$. C = Control; S = Saponins; F = Flavonoids; T = Tannins. Source: Kendall and Michael, 2010.

gene expression when compared with control; meanwhile, the aqueous extract at 30 mg/kg (0.525±0.05) caused a slight repression in GLUT4 gene expression in the liver of rats, whereas aqueous extract at 100 mg/kg (0.545±0.05) as well as the ethanol extract at 30 mg/kg bw (0.545±0.05) showed no significant difference when compared with control (0.55±0.02).

Saponins (0.95±0.05), flavonoids (0.75±0.03), and tannins (0.81±0.02) fractions of *C. citratus* at 30 µg/kg bw levels did not significantly alter KCJN5 gene expression as the levels observed were statistically similar to control (0.97±0.05).

DISCUSSION

Insulin affects fuel metabolism by the stimulation of glycolysis, glycogenesis, and lipogenesis as well as inhibition of gluconeogenesis, glycogenolysis, and lipolysis (Zhao et al., 2017). The mechanism of insulin action on carbohydrate metabolism occurs when glucose concentration is higher, such as after eating (Najjar and Perdomo, 2019). Insulin secreted by β-cells into the blood stream promotes glycolysis to lower elevated glucose levels by removal of glucose from blood stream to most body cells causing its storage, and used by almost all tissues of the body directly (Giugliano et al., 2019). Alteration or reduction in the activities of insulin termed insulin resistance often results to type 2 diabetes (Demircik et al., 2019), and has been linked with both genetic and environmental factors (Giugliano et al., 2019). This may lead to blockage in the biochemical pathways, by which glucose uptake and metabolism by the cells occurs (Kuzulugil et al., 2019; Athyros et al., 2020).

The relationship between insulin and glucagon like-peptide-1 (GLP-1) has been established and explained through scientific research-based evidences. GLP-1, as an incretin, functions by potentiating the secretion of insulin after meal ingestion in a glucose-dependent manner, exerting its insulinotropic actions through distinct G-protein-coupled receptors that is highly expressed on

islet β-cells (Nauck and Meier, 2019). The increase in GLP-1 gene expression by *C. citratus* powder administered rat complied with the reports of Steinert et al. (2017) and Reimann and Gribble (2016), who explained the secretory controls and physiological roles of GLP-1 in eating and glycemia in health, obesity.

The mechanism of action of GLP-1, a product of the pre-proglucagon gene, is often based on its released from L cells in the intestine upon food intake and potently activate the release of insulin from pancreatic ß-cells in a glucose-dependent manner in both normal and type 2 diabetic subjects (Modvig et al., 2019). Type 2 diabetes mellitus is usually as a result of defect in insulin secretion and peripheral insulin resistance, thus, therapies based on the incretin, glucagon-like peptide 1 (GLP-1) may be important treatment options for type 2 diabetes (Psichas et al., 2017). This is because they act through a variety of complementary mechanisms, through an increase in the amount of insulin released from beta cells in the pancreas following ingestion of food. Interestingly, a number of additional effects of GLP-1 on the pancreas have been observed to include stimulation of insulin biosynthesis and growth of ß-cell mass (Psichas et al., 2017). Thus, GLP-1 may play a vital role in both glycaemic treatment of type 2 diabetes and potentially prevent or delay the progression of diseases.

The current understanding is that GLP-1 stimulates insulin exocytosis. Christiansen et al. (2019) reported that GLP-1 resulted in the increase in immunoreactive insulin content, by lowering postprandial hyperglycemia via three independent mechanisms, which include increased insulin secretion, inhibition of glucagon release, and inhibition of gastrointestinal motility. GLP-1 treatment corrects several of the fundamental defects in diabetic ß-cell function through its insulinotropic activities (Holst et al., 2019). It can be said that the activation of GLP-1 genes by *C. citratus* powder and ethanol extracts may produce hypoglycaemic/antidiabetic effects by causing significant improvements in glycemic control through the release of insulin.

The progressive effect of the whole plant, solvent extracts, and phytochemical fractions of *C. citratus* on GLP-1 gene expression implies a progressive decline in the gene activation and activities. In fact, it can be deduced that the bioactive components that promote GLP-1 release reside outside the saponins, flavonoids, and tannins fractions. Several studies have corroborated the finding that specific biological activities of plant extracts are reduced when such extracts are fractionated further (Alema et al., 2020; Meresa et al., 2017; Taye et al., 2020). It can therefore be concluded that the whole plant of *C. citratus* potentiates GLP-1 gene up-regulation better than its extracts or individual phytochemical fractions. The significant increase in the expression of insulin gene occasioned by the administration of aqueous and ethanol extracts of *C. citratus* attested to the insulinotrophic effect of this plant. The flavonoid enriched fractions of this plant also caused significant increase in insulin gene expression; while saponins and tannins did not alter the expression of this gene. This clearly implies that *C. citratus* may initiate and potentiate hypoglycaemia by improving insulin secretion, an effect that is still retained in the flavonoid fractions (Reyes et al., 2017; Leonidas et al., 2017). It is not farfetched to suggest that the antioxidant properties of flavonoids may confer protective effects on pancreatic beta cells and thus optimize its ability to produce enough insulin needed by the body (Abotaleb et al., 2018; Kawser et al., 2016; Tanveer et al., 2017).

This study, also investigated the effect of *C. citratus* on GLUT-4 gene expression in liver cells in order to elucidate the molecular basis of its anti-diabetic potential. The transportation of glucose down its concentration gradient is mediated by members of the facilitative glucose transporter (GLUT) families, which are often expressed on the plasma membrane of all cells (Vargas et al., 2021). Insulin increases glucose uptake rate majorly by stimulating the translocation of the GLUT-4 isoforms from intercellular pools to the surface of cell membrane by increasing rate of glucose transport (Rashmi and Manonmani, 2020). So, it can be said that the effect(s) of *C. citratus* (especially the 100 mg/kg bw ethanol extract) to up regulate GLUT-4 may be useful for treatment of insulin insufficiency or insulin resistance. This up-regulation of the GLUT-4 gene by *C. citratus* ethanol extract leads to increased expression of GLUT-4 gene in treated animals, which provides strong indications that this extract will not only boost insulin level but will provide the channel for efficient tissue assimilation and usage of glucose.

These findings are in agreement with the results of Sleman et al. (2018) and Rashmi and Manonmani (2020), who reported that *Teucrium polium* extracts stimulate GLUT4 translocation to the plasma membrane in rats. Any disorder in KCNJ5 expression results to glucose intolerance or overt diabetes mellitus (Vargas et al., 2021), since the product of this gene increases insulin secretion.

Conclusion

The administration of *C. citratus* potentiated several insulinotrophic pathways. The ability of this plant to up-regulate the expression of insulin, GLP-1, and GLUT-4 genes indicates several therapeutic interventions for hyperglycaemia. General comparism of the results obtained from the different administered samples suggests a decline in insulinotrphic effects from whole plants to whole solvent extracts to isolated phytochemical. It could therefore be concluded, at least for GLP-1 gene expression, that the entire array of phytochemicals present in the whole plant may produce better insulonotrophic effect.

CONFLICT OF INTERESTS

The authors have not declared any conflict of interests.

ACKNOWLEDGEMENT

The authors appreciate the support from the Government of the Federal Republic of Nigeria through the Tertiary Education TrustFund (TETFUND) grant, PV. No 090435/24.

REFERENCES

Abotaleb M, Samuel SM, Varghese E, Varghese S, Kubatka P, Liskova A, Busselberg D (2018). Flavonoids in Cancer and Apoptosis. Cancers (Basel) 11:28.

Ajayi EO, Sadimenko AP, Afolayan AJ (2016). GC-MS evaluation of *Cymbopogon citratus* (DC) Stapf oil obtained using modified hydrodistillation and microwave extraction methods. Food Chemistry 209:262-266.

Alema NM, Periasamy G, Sibhat GG, Tekulu GH, Hiben MG (2020). Antidiabetic activity of extracts of *Terminalia brownii* Fresen. Stem bark in mice. Journal of Experimental Pharmacology 12:61-71.

Al-Lawati JA (2017). Diabetes mellitus: A local and global public health emergency! Oman Medical Journal 32:177-179.

Athyros VG, Polyzos SA, Kountouras J, Katsiki N, Anagnostis P, Doumas M, Mantzoros CS (2020). Non-alcoholic fatty liver disease treatment in patients with type 2 diabetes mellitus; New kids on the block. Current Vascular Pharmacology 18(2):172-181.

Baggio LL, Yusta B, Mulvihill EE, Cao X, Streutker CJ, Butany J, Cappola TP, Margulies KB, Drucker DJ (2018). GLP-1 receptor expression within the human heart. Endocrinology 159:1570-1584.

Bello OM, Jagaba SM, Bello OE, Ogbesejana AB, Dada OA, Adetunji CO, Abubakar SM (2019). Phytochemistry, pharmacology and perceived health uses of non-cultivated vegetable Cyphostemma adenocaule (Steud. ex A. Rich.) Desc. ex wild and R.B. Drumm: A review. Scientific African 2:e00053.

Burmeister MA, Ayala JE, Smouse H, Landivar-Rocha A, Brown JD, Drucker DJ, Stoffers DA, Sandoval DA, Seeley RJ, Ayala JE (2017). The hypothalamic glucagon-like peptide 1 receptor is sufficient but not necessary for the regulation of energy balance and glucose homeostasis in mice. Diabetes 66:372-384.

Cho NH, Shaw JE, Karuranga S, Huang Y, da Rocha Fernandes JD, Ohlrogge AW, Malanda B (2018). IDF Diabetes Atlas: Global estimates of diabetes prevalence for 2017 and projections for 2045. Diabetes Research and Clinical Practice 138:271-281.

Christiansen CB, Trammell SAJ, Albrechtsen NJW, Schoonjans K, Albrechtsen R, Gillum MP, Kuhre RE., Holst JJ (2019). Bile acids drive colonic secretion of glucagon-like-peptide 1 and peptide-YY in rodents. American Journal of Physiology-Gastrointestinal and Liver Physiology 316:G574-G584.

Coelho M, Rocha C, Cunha LM, Cardoso L, Alves L, Lima RC, Pintado M (2016). Influence of harvesting factors on sensory attributes and phenolic and aroma compounds composition of *Cymbopogon citratus* leaves infusions, Food Research International 89:1029-1037.

Demircik F, Kirsch V, Ramljak S, Vogg M, Pfützner AH, Pfützner A (2019). Laboratory evaluation of linearity, repeatability, and hematocrit interference with an internet-enabled blood glucose meter. Journal of Diabetes Science and Technology 13(3):514-521.

Di Meo S, Reed TT, Venditti P, Victor VM (2016). Role of ROS and RNS Sources in Physiological and Pathological Conditions. Oxidative Medicine and Cellular Longevity.

Di Meo S, Reed TT, Venditti P, Victor VM (2018) Harmful and Beneficial Role of ROS 2017. Oxid. Med. Cell Longev.

Drucker DJ, Habener JF, Holst JJ (2017). Discovery, characterization, and clinical development of the glucagon-like peptides. Journal of Clinical Investigation 127:4217-4227.

Einarson TR, Acs A, Ludwig C, Panton UH (2018). Prevalence of cardiovascular disease in type 2 diabetes: A systematic literature review of scientific evidence from across the world in 2007-2017. Cardiovascular Diabetology 17(1):1-9.

Giugliano D, De Nicola L, Maiorino MI, Bellastella G, Esposito K (2019). Type 2 diabetes and the kidney: Insights from cardiovascular outcome trials. Diabetes, Obesity and Metabolism (8):1790-1800.

Holst JJ, Albrechtsen NJW, Rosenkilde MM, Deacon CF (2019). Physiology of the incretin hormones, GIP and GLP-1—regulation of release and posttranslational modifications. Comprehensive Physiology 9:1339-1381

Hou Y, Ernst SA, Heidenreich K, Williams JA (2016). Glucagon-like peptide-1 receptor is present in pancreatic acinar cells and regulates amylase secretion through cAMP. American Journal of Physiology-Gastrointestinal and Liver Physiology 310(G):26-33.

International Diabetes Federation (IDF) (2020). Diabetes facts and figures. IDF Diabetes atlas, 9th edition.

Kawser Hossain M, Abdal Dayem A, Han J, Yin Y, Kim K, Kumar Saha S, Cho SG (2016). Molecular mechanisms of the anti-obesity and anti-diabetic properties of flavonoids. International Journal of Molecular Sciences 17:569.

Klip A, McGraw TE, James DE (2019). Thirty sweet years of GLUT4. Journal of Biological Chemistry 294:11369-11381.

Kuzulugil D, Papeix G, Luu J, Kerridge RK (2019). Recent advances in diabetes treatments and their perioperative implications. Current Opinion in Anaesthesiology 32(3):398-404.

Lauritano C, Ianora A (2016). Marine organisms with anti-diabetes properties. Marine Drugs 14:220

Lawal OA, Ogundajo AL, Avoseh NO, Ogunwande IA (2017). *Cymbopogon citratu*. InMedicinal Spices and Vegetables from Africa 2017 Jan 1 (pp. 397-423). Academic Press.

Leonidas DD, Hayes JM, Kato A, Skamnaki VT, Chatzileontiadou DS, Kantsadi AL, Stravodimos GA (2017). Phytogenic polyphenols as glycogen phosphorylase inhibitors: the potential of triterpenes and flavonoids for glycaemic control in type 2 diabetes. Current Medicinal Chemistry 24:384-403

Meresa A, Gemechu W, Basha H (2017). Herbal medicines for the management of diabetic mellitus in Ethiopia and Eretria including their phytochemical constituents. American Journal of Advanced Drug Delivery 5(1):1-25

Modvig IM, Kuhre RE, Holst JJ (2019). Peptone-mediated glucagon-like peptide-1 secretion depends on intestinal absorption and activation of basolaterally located calcium-sensing receptors. Physiological Reports 7(8):e14056.

Najjar SM, Perdomo G (2019). Hepatic Insulin Clearance: Mechanism and Physiology. Physiology (Bethesda) 34(3):198-215.

Nauck MA, Meier JJ (2019). GIP and GLP-1: Stepsiblings rather than monozygotic twins within the incretin family. Diabetes 68(5):897-900.

Onoagbe IO, Esekheigbe A (1999). Studies on the anti-diabetic properties of *Uvaria Chamae* in streptozotocin-induced diabetic rabbits. Biokemistri 9:79-84.

Psichas A, Larraufie PF, Goldspink DA, Gribble FM, Reimann F (2017). Chylomicrons stimulate incretin secretion in mouse and human cells. Diabetologia 60:2475-2485.

Rashmi S. Manonmani H (2020). A triterpene glycoside fraction, TG from *Gymnema sylvestre* ameliorates insulin resistance by stimulating glucose uptake in 3T3L1 adipocytes and C2C12 skeletal muscle cells. Journal of Biosciences and Medicines 8(11):137-151.

Reimann F, Gribble FM (2016). Mechanisms underlying glucose-dependent insulinotropic polypeptide and glucagon-like peptide-1 secretion. Journal of Diabetes Investigation 7:13-19

Reyes J, Tripp-Reimer T, Parker E, Muller B, Laroche H (2017). Factors influencing diabetes self-management among medically underserved patients with type II diabetes. Global Qualitative Nursing Research 4:23-33.

Sleman K, Yoel S, Raed A, Bashar S, Shoshana B, Thomas L, Guy C, Hilal Z (2018). *Teucrium polium* extracts stimulate GLUT4 translocation to the plasma membrane in L6 muscle cells. Advancement in Medicinal Plant Research 6(1):1-8.

Steinert RE, Feinle-Bisset C, Asarian L, Horowitz M, Beglinger C, Geary N, Ghrelin CCK (2017). GLP-1 and PYY (3-36): Secretory controls and physiological roles in eating and glycemia in health, obesity, and

after RYGB. Physiological Reviews 97:411-463
Subramanian SS, Nagarjan S (1969). Flavonoids of the seeds of *Crotolaria retusa and Crotolaria strata.* Current Science 38:65-71
Tanveer A, Akram K, Farooq U, Hayat Z, Shafi A (2017). Management of diabetic complications through fruit flavonoids as a natural remedy. Critical Reviews in Food Science and Nutrition 57:1411-1422.
Taye GM, Bule M, Gadisa DA, Teka F, Abula T (2020). *In vivo* antidiabetic activity evaluation of aqueous and 80% methanolic extracts of leaves of *Thymus schimperi* (Lamiaceae) in alloxan-induced diabetic mice. Diabetes, Metabolic Syndrome and Obesity: Targets and Therapy 13:3205-3212.
Vargas E. Podder V, Carrillo Sepulveda MA (2021). Physiology, Glucose Transporter Type 4. Treasure Island: StatPearls Publishing.
Vlavcheski F, Baron D, Vlachogiannis IA, MacPherson REK, Tsiani E (2018). Carnosol increases skeletal muscle cell glucose uptake *via* AMPK-dependent GLUT4 glucose transporter translocation. Critical Reviews in Food Science and Nutrition 19:13-21
Wall ME, Wani MC, Brown DM (1996). Effect of tannins on screening of plant extracts for enzyme inhibitory activity and techniques for their removal. Phytomedicine 3:281-285.
Wang C, Wang S, Yang H, Xiang Y, Wang X, Bao C, Zhu L, Tian H, Qu D (2021). A Light-Operated Molecular Cable Car for Gated Ion Transport. Angewandte Chemie 133(27):14962-14966
Woo WS, Shin KH, Kang SS (1980). Chemistry and Pharmacology of Flavone -C- Glycoside from *ziziphus* seeds. Korean Journal of Pharmacognosy 11(3-4):141-148.
World Health Organisation (WHO) (2019). "Diabetes Fact sheet N°312".
World Health Organisation (WHO) (2021). "Diabetes Fact sheet N°312".
World Health Organization (WHO) (2020). About Diabetes mellitus.
Wu P, Gao ZX, Zhang DD, Su XT, Wang WH, Lin DH (2019). Deletion of Kir5.1 impairs renal ability to excrete potassium during increased dietary potassium intake. Journal of the American Society of Nephrology 30(8):1425-1438.
Zhang Y, Sun B, Feng D, Hu H, Chu M, Qu Q, Tarrasch JT, Li S, Sun Kobilka T, Kobilka BK, Skiniotis G (2017). Nature 546:248-253
Zhao L, Wang L, Zhang Y, Xiao S, Bi F, Zhao J, Gai G, Ding J (2017). Glucose oxidase-based glucose-sensitive drug delivery for diabetes treatment. Polymers (Basel) 29 9(7):255.
Zheng Y, Ley SH, Hu FB (2018). Global aetiology and epidemiology of type 2 diabetes mellitus and its complications. Nature Reviews Endocrinology 14:88-98.

Related Journals: